Draft version June 16, 2024
Typeset using LaTeX default

BSN: The First Photometric Study of Ten Contact Binary Systems from the Northern and Southern Hemispheres

Atila Poro,[1,*] Kai Li,[2,†] Raul Michel,[3] Angel Castro,[3] Eduardo Fernández Lajús,[4,5] Li-Heng Wang,[2] Fahri Alicavus,[6,7] Jean-François Coliac,[8] Yasemin Aladağ,[9] and Ailar Alizadehsabegh[10]

[1] *Astronomy Department of the Raderon AI Lab., BC., Burnaby, Canada*
[2] *Shandong Key Laboratory of Optical Astronomy and Solar-Terrestrial Environment, School of Space Science and Physics, Institute of Space Sciences, Shandong University, Weihai, Shandong 264209, People's Republic of China*
[3] *Observatorio Astronómico Nacional, Universidad Nacional Autónoma de México, Apartado Postal 877, Ensenada C.P. 22800, B.C., México*
[4] *Instituto de Astrofísica de La Plata (CCT La Plata-CONICET-UNLP), La Plata, Argentina*
[5] *Facultad de Ciencias Astronómicas y Geofísicas, Universidad Nacional de La Plata, Paseo del Bosque, B1900FWA, La Plata, Argentina*
[6] *Çanakkale Onsekiz Mart University, Faculty of Arts and Sciences, Department of Physics, 17020, Çanakkale, Türkiye*
[7] *Çanakkale Onsekiz Mart University, Astrophysics Research Center and Ulupnar Observatory, 17020, Çanakkale, Türkiye*
[8] *Double Stars Committee, Société Astronomique de France, Paris, France*
[9] *Space Science and Solar Energy Research and Application Center (UZAYMER), University of Çukurova, 01330, Adana, Türkiye*
[10] *Department of Photonics, University of Tabriz, Tabriz, Iran*

ABSTRACT

Photometric observations were made with standard filters in four observatories for ten contact binary systems. We analyzed the orbital period variations of the systems. We concluded that the reduction in the orbital period of the J05, LO Psc, and N49 systems is caused by Angular Momentum Loss (AML) rather than mass transfer. The first light curve analysis was performed with the PHysics Of Eclipsing BinariEs (PHOEBE) Python code and Markov chain Monte Carlo (MCMC). We discuss the relationship between mass ratio results with spectroscopic and photometric data as well as total and partial eclipse systems. We have shown that the samples used cannot confirm conclusive results in obtaining more accurate mass ratios in total eclipsing systems from photometric data. We also compared our mass ratio findings from MCMC to a recent method that estimates mass ratios from the light curve's third derivative. We also discussed this new mass ratio estimate method for photometric data and made some suggestions. Eighteen relationships between parameters and empirical relationships were used to examine the target systems' outcomes. According to the light curve analysis and estimation of absolute parameters, systems BE Mus and J07 are A-subtypes, and the others are W-subtypes.

Keywords: Close binary stars (254); CCD photometry(208); Fundamental parameters of stars (555); Astronomy data analysis(1858)

1. INTRODUCTION

There remain many significant questions about binary systems after decades of investigations. They are crucial objects for studying the structure and formation of stars, examining stellar evolution theories, and figuring out the physical characteristics of stars (Qian 2003, Yakut & Eggleton 2005, Li et al. 2007, Eker et al. 2008, Eggleton 2012, Poro et al. 2024b).

Based on the general shape of the light curves, eclipsing binary systems were initially categorized into three types: Algol, β Lyrae, and W Ursae Majoris (W UMa) types. However, a more appropriate category was provided by Kopal (1959), which had a more precise description of the state of these eclipsing systems. Therefore, based on Roche geometry, binaries were classified as detached, semi-detached, and contact systems.

* atilaporo@bsnp.info
† kaili@sdu.edu.cn

W UMa-type eclipsing contact binary systems contain two stars sharing a common convective envelope (Lucy 1968a, Lucy 1968b). These stars are around the main sequence, with spectral types of F to K. Contact binary systems show a continuous light variation and a small difference between the depths of the two minima (Qian et al. 2014). The temperatures of two stars in contact systems are close (Kuiper 1941), and the higher the fillout factor, the more equilibrium can be expected. According to the Latković et al. (2021) study, if both conditions, including a higher orbital period than 0.5 days and an effective temperature of 7000, exist, that system will not be classified as a W UMa-type. Therefore, it can be found in a simple search that most of the systems studied so far have an effective temperature range of about 3500 K to 7200 K.

Contact binary systems have a short orbital period, mostly around 0.2 to 0.6 days. Based on the Rucinski (1992) study, contact binaries have a sharp orbital period cutoff at about 0.22 days. Then, other systems were discovered with even shorter orbital periods (e.g., Weldrake et al. 2004, Drake et al. 2014a, Jiang et al. 2015). The reasons for the orbital period cutoff are far from clear yet. Thanks to various databases like Variable Star indeX (VSX), Large Sky Area Multi-Object Fiber Spectroscopic Telescope (LAMOST), Catalina Surveys Data Release-1 (CSDR1), the General Catalogue of Variable Stars (GCVS), and the worldwide photometric surveys, statistics reviews on the period distribution of contact binaries were carried out (Zhang & Qian 2020). The studies show that a sharp decline at about 0.22 days can be recognized (Li et al. 2020). Despite the theoretical studies, it is necessary to increase and analyze the number of contact systems that are in the orbital period cut-off range. On the other hand, the accurate determination of the orbital period can have an impact on other statistical and experimental parameter relationships/theories for determining the absolute parameters of stars, such as mass (Qian 2003, Poro et al. 2022a).

Contact binaries are divided into A and W subtypes (Binnendijk 1970). The more massive component is a hotter star in the A-subtype, and if the less massive component has a higher effective temperature, it is classified as a W-subtype. Specifying the subtype depends on which star we consider primary. However, Csizmadia & Klagyivik (2004) suggested the B subtype for W UMa contact binaries. B-subtype systems' temperature difference between components is more than 1000 K, and they are also referred to as poor thermal contact binaries (Rucinski 2000). These categorizations for subtypes are still under discussion, and in some cases, it is challenging to distinguish subtypes.

In this study, ten contact binary systems from the southern and northern hemispheres were investigated. We used ground-based photometric observations, along with TESS data for some systems. The observations were conducted by four observatories in the Binary Systems of South and North (BSN[1]) project. The first light curve analysis and estimating the absolute parameters of the target binary systems have been the main parts of this work. Finally, a discussion and conclusion on the systems are presented.

2. TARGET SYSTEMS

We have analyzed ten binary stars classified in the catalogs as contact systems. These targets include BE Mus, CSS J050736.0+214218 (hereinafter J05), CSS J072227.8+443027 (hereinafter J07), CSS J081118.7+320828 (hereinafter J08), LO Psc, NSVS 4908885 (hereinafter N49), NSVS 6527318 (hereinafter N65), OT UMa, PU Vir, and V0801 And. A general introduction and some of their specifications are provided:

• BE Mus: Guthnick & Prager (1933) presented an ephemeris for this system for the first time, and they announced the orbital period as 0.3369219 days. Additionally, the Guthnick & Prager (1933) study reported a maximum apparent magnitude of $V_{max} = 13.3^{mag.}$ for BE Musca. The GCVS (Malkov et al. 2006) and the Catalogue of Eclipsing Variables (Avvakumova et al. 2013) classify BE Mus as a Southern hemisphere contact binary system. Gaia DR3 reported 5961 K for BE Mus's effective temperature.

• J05: This binary system was discovered by the CSDR1 (Drake et al. 2014b). J05 is observed in the Taurus constellation. The CSDR1 and ASAS-SN catalogs reported orbital periods of 0.2339980 and 0.2094278 days, respectively. In addition to the difference in the orbital period in catalogs CSDR1 and ASAS-SN, they reported the mean magnitude in the V filter as $V_{CSDR1} = 14.78(25)^{mag}$ and $V_{ASAS-SN} = 16.03(40)^{mag}$. Looking at the results of TESS ($V_{TESS} = 16.199(355)^{mag}$), it seems that the results of ASAS-SN are more reliable. Gaia DR3 and TESS database determined $T_{GaiaDR3} = 4136$ K and $T_{TESS} = 4001(123)$ K for J05 as a low-temperature binary system.

[1] https://bsnp.info/

• J07: The Lynx constellation is where this target system is located. The CSDR1 discovered J07 and reported an orbital period of 0.226522 days. J07 was included in the Asteroid Terrestrial-impact Last Alert System (ATLAS) REFCAT2 catalog (Tonry et al. 2018), and its apparent magnitudes were given in the g, r, i, z, J, H, and K bands. The Zwicky Transient Facility (ZTF) catalog also classifies J07 as a contact binary system (Chen et al. 2020). The effective temperature of J07 is reported by the Gaia DR3 as 4678 K.

• J08: This binary system is located in the Cancer constellation. J08 was discovered by the CSDR1, and an orbital period of 0.246884 days was determined for it. Catalogs ATLAS, ZTF, and ASAS-SN have reported J08 as a contact binary system. J08 was included in a sample of 9380 contact binaries using the Catalina Real-Time Transient Survey Variables Sources Catalogue (Marsh et al. 2017). According to Marsh et al. (2017), the system's effective temperature is 4667 K, while Gaia DR3 and TESS reported 4904 K and 4504(107), respectively.

• LO Psc: This binary system was discovered by the ROTSE-I telescope and included in a catalog of 1022 bright contact binary stars presented in the Gettel et al. (2006) study. The study by Hoffman et al. (2009) classified LO Pisces as a contact binary system. Terrell et al. (2012) reported a BVR_cI_c survey of 606 W UMa binary stars and presented $B-V$, $V-R_c$, R_c-I_c, and $V-I_c$. They defined V_{max} as 10.94^{mag} and an orbital period of 0.3455752 days. TESS has reported a temperature of 5554 K for LO Psc; however, Gaia DR3 has not specified any value.

• N49: This system is located in the Ursa Major constellation. CSDR1 was discovered in this system. N49 is classified as a contact binary in the ASAS-SN, VSX, ZTF, and ATLAS catalogs. The VSX database reported $V_{max} = 13.45^{mag}$ for this system. The ZTF variables catalog presented a t_0 and orbital period of 0.2441638 days for N49. The temperatures of the N49 binary system have been determined to be 4395 K in the Gaia DR3 and 4386(129) K in the TESS database.

• N65: This target is in the Triangulum constellation. N65 was identified in the Northern Sky Variability Survey as a W UMa-type with an orbital period of 0.26417 days (Hoffman et al. 2009). For this system, the VSX database presented $V_{max} = 13.24^{mag}$. N65 is also classified as a contact binary system in the ZTF, ASAS-SN, and ATLAS catalogs. Gaia DR3 and TESS reported the effective temperature of the system as 5243 K and 5439(186) K, respectively.

• OT UMa: An ephemeris provided by the Peremennye Zvezdy Prilozhenie (PZP) database (Khruslov 2007). The General Catalogue of Variable Stars (GCVS) and VSX reported the same $V_{max} = 12.22^{mag}$ for OT Ursa Major. Many catalogs such as ASAS-SN, VSX, GCVS, WISE, and ZTF have classified OT UMa as a contact binary system. The ZTF variables catalog presented a t_0 and an orbital period of 0.3160738 days for this target. The reported Gaia DR3 effective temperature for OT UMa is 5769 K, and this parameter's value is 5643(142) K from the TESS database.

• PU Vir: This target was found by L. Bernasconi to be a variable (Rinner et al. 2003). The Rinner et al. (2003) study presented the first ephemeris with an orbital period of 0.2562555(14) days, and they recognized PU Virgo as a contact system. Additionally, the GCVS, ASAS-SN, and VSX databases classified PU Vir as a contact binary star. The ASAS variable stars in the southern hemisphere (ASAS3) catalog reported $V_{max} = 12.10^{mag}$. An effective temperature of 4967 K by Gaia DR3 and 5107(108) K by TESS are reported for this system.

• V0801 And: TAROT robotic observatory in France was discovered V0801 And with an orbital period of 0.266628 days (Damerdji et al. 2007). V0801 Andromeda was classified as a contact binary system by the ASAS-SN, VSX, ATLAS, and GCVS catalogs. The GCVS catalog reported $V_{max} = 11.95^{mag}$ for this system. Gaia DR3 and TESS presented an effective temperature for this system of 4890 K and 5009(193) K, respectively.

3. OBSERVATION AND DATA REDUCTION

Photometric observations and data reductions were made with different standard filters for ten target systems in four observatories in the Northern and Southern Hemispheres. These observations were carried out on 13 nights during the years 2023 and 2024 (Table 2).

We considered the airmass with a formula from the Hiltner (1962) study and a Python code based on the Astropy package (Astropy Collaboration et al. 2013) for all of the ground-based observations. Additionally, airmass was applied to the light curves, and the flux was normalized using the AstroImageJ (AIJ) software (Collins et al. 2017).

Table 1 contains the coordinates and distance from Gaia DR3 (Gaia Collaboration et al. 2023), the orbital period of the target systems from catalogs, and V_{max} determined from our observations. The observational information for each of the systems is presented in Table 2. Table 3 lists the comparisons and checks stars and their coordinates from Gaia DR3.

3.1. *CASLEO Observatory*

The observations of the BE Mus and PU Vir were made using the 2.15-meter Jorge Sahade (JS) telescope at the Complejo Astronomico El Leoncito (CASLEO) Observatory, Argentina (69°18′ West, 31°48′ South, 2552 m above sea level). A CCD Versarray 2048B, Roper Scientific, Princeton Instruments, and standard BVR_cI_c filters were employed. Also, the scale of 0.15 asec/pix, and binning 5×5 were used for observations.

The APPHOT photometry package of the Image Reduction and Analysis Facility[2] (IRAF) was used for CCD reduction and aperture photometry (Tody 1986). These processes were conducted using bias and flat-field images.

3.2. *SPM Observatory*

The five binary systems J05, J07, J08, N49, and N65 were observed at the San Pedro Martir (SPM) Observatory in Mexico. This observatory is located at longitude 115° 27' 49" West, latitude 31° 02' 39" North, and altitude of 2830 m above sea level. The following equipment was utilized for the observations: A 0.84-meter Ritchey-Chretien telescope ($f/15$), a Mexman filter wheel, a Spectral Instruments CCD detector (e2v CCD42-40 chip with $13.5 \times 13.5\mu2$ pixels, the gain of $1.39e-/$ ADU, and readout noise of $3.54e-$), and BVR_cI_c standard filters.

All the images were processed using IRAF[3] routines (Tody 1986). Images were bias subtracted, flat field corrected, and aligned before the instrumental magnitudes were computed with the standard aperture photometry method using an aperture of 1.5 times the average FWHM of each object's images.

3.3. *UZAYMER Observatory*

The observations of LO Psc were carried out by a 0.5-meter Ritchey-Chretien RC 500/4000 Pro RC SGA OTA ($f/8$) telescope at the UZAYMER Observatory, Çukurova University, Adana, Türkiye (longitude 35° 21' 19" North, latitude 37° 03' 35" East and altitude of 130 m). We used a Finger Proline Instruments PL16803 type CCD with 4096×4096 pixels and a $9\mu m$ pixel size. The CCD temperature average during observations was -30°C. Observations were conducted using standard filters V and R_c.

The standard process was employed for performing basic data reduction using bias, dark, and flat-field on the raw CCD images. We aligned, reduced, and plotted raw images with AIJ software (Collins et al. 2017).

3.4. *OABAC Observatory*

The OT UMa and V0801 And binary systems were observed at the OABAC observatory in Marseille, France (longitude 43° 18' 54" North and latitude 05° 27' 56" East). We used a Newton 200mm ($f/4$) telescope with a field corrector in the observation process.

An ASI ZWO 183MM Pro with standard VI_c filters for OT UMa and an ASI ZWO 533MM pro CCDs with standard BVR_c filters were applied for V0801 And. The average CCD temperature for both systems' observations was 0°C.

We employed FotoDif[4] and Siril[5] software for the standard data reduction process, using dark, bias and flat-field on the images.

3.5. *TESS Observations*

NASA launched the Transiting Exoplanet Survey Satellite (TESS) in 2018 with the goal of discovering exoplanets (Ricker et al. 2010, Stassun et al. 2018). Four wide-field cameras on this space telescope allow it to observe different parts of the sky. TESS observes a designated region of the sky during each sector for 27.4 days. We used time-series available TESS data for the BE Mus, J08, LO Psc, N49, N65, OT UMa, and V0801 And binary systems. 'TESS:T' is used as a passband in these systems' light curve analysis process, covering a broadband wavelength range of 600–1000 nm (Ricker et al. 2015a). Table 4 lists the TESS sectors used in this study.

[2] http://iraf.noao.edui

[3] IRAF is distributed by the National Optical Observatories, operated by the Association of Universities for Research in Astronomy, Inc., under a cooperative agreement with the National Science Foundation.

[4] http://www.astrosurf.com/orodeno/fotodif/

[5] https://siril.org/

Table 1. Specifications of the target systems. Coordinates and distance come from the Gaia DR3.

System	2MASS	RA.°(J2000)	Dec.°(J2000)	d(pc)	P(day)/Source	V_{max}
BE Mus	012210592-6630324	185.274399	-66.509041	502.43(3.45)	0.3369275/ASAS-SN	13.56(17)
J05	05073605+2142186	76.900318	21.705154	308.42(3.16)	0.2094278/ASAS-SN	16.13(21)
J07	07222780+4430280	110.615799	44.507746	673.62(11.44)	0.2265227/ASAS-SN	15.12(11)
J08	08111879+3208279	122.828232	32.141005	373.27(37.40)	0.2468829/ASAS-SN	14.40(15)
LO Psc	00532822+2536229	13.367713	25.606332	255.64(1.46)	0.345567/VSX	11.57(9)
N49	10202456+4306412	155.102411	43.111422	287.70(1.59)	0.2441642/ASAS-SN	13.99(10)
N65	02265165+2935160	36.715283	29.587658	412.36(4.17)	0.264175/ASAS-SN	13.53(9)
OT UMa	08192313+6612364	124.846027	66.209919	359.89(1.62)	0.316067/VSX	12.49(8)
PU Vir	012394855-0226216	189.952494	-2.439391	204.09(0.99)	0.2562555/ASAS-SN	12.37(13)
V0801 And	02000913+4302429	30.037984	43.045356	234.71(1.10)	0.266655/VSX	12.33(11)

Table 2. Specifications of the ground-based observations.

System	Observation(s) Date	Filter	Exposure time(s)	Binning	Observatory
BE Mus	2024(Mar. 10)	BVR_cI_c	B(60), V(20), R_c(20), I_c(15)	5×5	CASLEO
J05	2023(Dec. 7)	BVR_cI_c	B(20), V(10), R_c(7), I_c(7)	2×2	SPM
J07	2024(Jan. 27)	BVR_cI_c	B(60), V(30), R_c(10), I_c(10)	2×2	SPM
J08	2024(Jan. 30)	BVR_cI_c	B(60), V(30), R_c(10), I_c(10)	2×2	SPM
LO Psc	2023(Oct. 13), 2023(Oct. 23)	VR_c	V(180), R_c(120)	2×2	UZAYMER
N49	2024(Jan. 26)	BVR_cI_c	B(60), V(30), R_c(10), I_c(10)	2×2	SPM
N65	2023(Nov. 22)	VR_cI_c	V(120), R_c(60), I_c(30)	2×2	SPM
OT UMa	2023(Fab. 10), 2023(Jan. 26)	VI_c	V(30), I_c(30)	4×4	OABAC
PU Vir	2024(Mar. 8)	BVR_cI_c	B(30), V(10), R_c(8), I_c(8)	5×5	CASLEO
V0801 And	2023(Nov. 15), 2023(Nov. 17)	BVR_c	B(60), V(60), R_c(60)	4×4	OABAC

TESS data is available at the Mikulski Space Telescope Archive (MAST)[6]. TESS-style curves were extracted from the MAST using the LightKurve[7] code. The data was detrended using the TESS Science Processing Operations Centre (SPOC) pipeline (Jenkins et al. 2016).

4. ORBITAL PERIOD VARIATIONS

We tried to collect as many eclipsing times as possible from photometric surveys, such as the All-Sky Automated Survey for SuperNovae (ASAS-SN; Shappee et al. 2014; Jayasinghe et al. 2018), the Zwicky Transient Facility (ZTF; Bellm et al. 2019; Masci et al. 2019), the Transiting Exoplanet Survey Satellite (TESS; Ricker et al. 2015b) and Wide Angle Search for Planets (SuperWASP; Butters et al. 2010), to assist in analyzing the orbital period variations of these ten targets. In addition, we also collected data from AAVSO and O-C Gateway. For TESS 2-min cadence data, SuperWASP, and AAVSO continuous observation data, we can directly calculate their eclipsing times. However, for the TESS 10-min and 30-min cadence data, ZTF, and ASAS-SN dispersed data, we used the period shift method suggested by Li et al. (2020) to obtain their eclipsing times. The Kwee & van Woerden (1956) method was applied to calculate the eclipsing times. Since both the Barycentric Julian Date in Barycentric Dynamical Time (BJD_{TDB}) and the Heliocentric Julian Date (HJD) are present in the data, we first used an online tool[8] to convert them all to BJD_{TDB}. The extracted eclipsing times are listed in Table 5 and appendix tables (Tables 1-10). Then, we calculated the O-C values using the equation 1,

[6] https://mast.stsci.edu/portal/Mashup/Clients/Mast/Portal.htmL

[7] https://docs.lightkurve.org

[8] https://astroutils.astronomy.osu.edu/time/hjd2bjd.html

Table 3. List of comparison and check stars in the observations. Coordinates come from the Gaia DR3.

System	Star Type	Star Name	RA.°(J2000)	DEC.°(J2000)
BE Mus	Comparison	2MASS J12211813-6631487	185.325515	-66.530221
BE Mus	Check	2MASS J12210234-6628597	185.259632	-66.483271
J05	Comparison	2MASS J05071636+2142372	76.818244	21.710333
J05	Check	2MASS J05073432+2142251	76.893094	21.707007
J07	Comparison	2MASS J07221823+4428562	110.575967	44.482269
J07	Check	2MASS J07221944+4430316	110.581053	44.508790
J08	Comparison	2MASS J08112004+3211048	122.833391	32.184544
J08	Check	2MASS J08110665+3211533	122.777705	32.198174
LO Psc	Comparison	TYC 1742-1501-1	13.436793	25.710722
LO Psc	Comparison	TYC 1742-1865-1	13.284319	25.555827
LO Psc	Check	TYC 1742-1793-1	13.491318	25.595772
N49	Comparison	2MASSJ10200956+4306382	155.039629	43.110361
N49	Check	2MASSJ10200956+4306382	155.074415	43.143527
N65	Comparison	2MASS J02270218+2933004	36.759139	29.550072
N65	Check	2MASS J02270206+2935412	36.758645	29.594799
OT UMa	Comparison	Gaia DR3 1093610793684777472	124.785057	66.362352
OT UMa	Check	Gaia DR3 1093555680664518656	124.844945	66.150794
PU Vir	Comparison	2MASS J12395360-0226443	189.973376	-2.445676
PU Vir	Comparison	SDSS J123954.17-022503.7	189.975830	-2.417822
PU Vir	Check	TYC 4948-1040-1	189.982445	-2.373548
V0801 And	Comparison	Gaia DR3 346511368669282048	30.023625	43.049184
V0801 And	Check	Gaia DR3 346524391010108544	29.920890	43.150740

Table 4. TESS data specifications used in this study.

System	TIC	TESS Sector	Exposure time(s)	Obs. Year
BE Mus	448018469	11, 37, 38, 64, 65	1426, 475, 475, 158, 158	2019, 2021, 2023
J08	165834549	20, 44, 45, 46, 47	1426, 475, 475, 475, 475	2019, 2020, 2021, 2022
LO Psc	13935976	17, 57	1426, 158	2019, 2022
N49	150229405	21, 48	1426, 475	2020, 2022
N65	21182129	18, 58	1426, 158	2019, 2022, 2023
OT UMa	99680466	20, 47, 60	1426, 475, 158	2020, 2022, 2023
V0801 And	291955609	18, 58	1426, 158	2019, 2022

$$BJD_{TDB} = BJD_{TDB0} + P \times E, \tag{1}$$

where BJD_{TDB} is the observational eclipsing times, BJD_{TDB0} is the initial primary eclipsing time, and P is the orbital period. The calculated results are displayed in Table ...., and the O-C diagram is shown in Figure 1. As we can see in this figure, four systems show linear variations, and the remaining six stars show parabolic variations. The equation 2 was used to fit the O-C diagrams,

$$O - C = \Delta T_0 + \Delta P_0 \times E + \frac{\beta}{2} E^2. \tag{2}$$

The fitted parameters are shown in 6. We found that three stars show a long-term increase in their orbital periods, while three stars show a long-term decrease in their orbital periods.

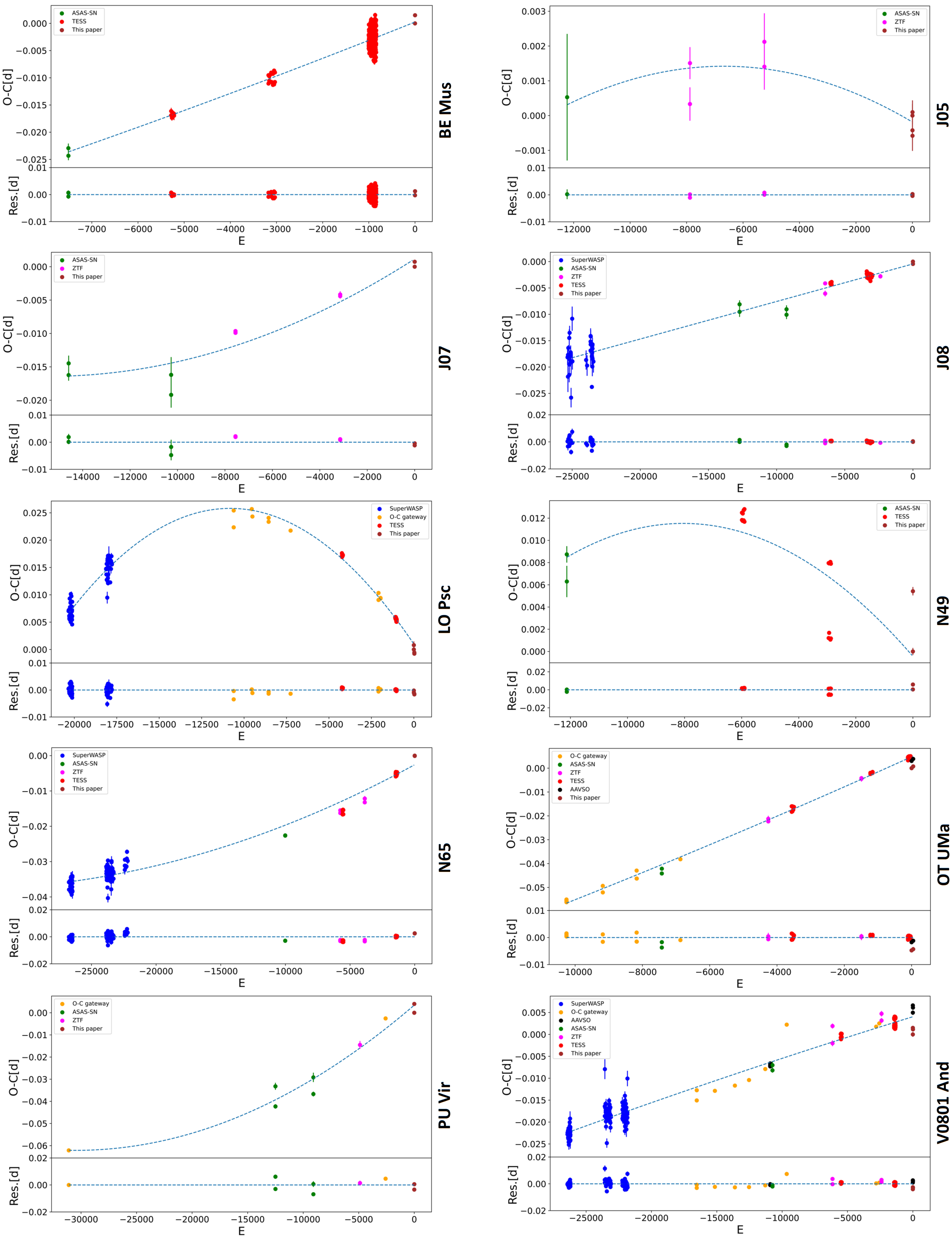

Figure 1. The O-C diagrams of the target binary systems.

Table 5. Extracted ground-based times of minima of our observations.

System	Min.(BJD_{TDB})	Error	Epoch	O-C
BE Mus	2460379.6489	0.0004	0	0.0000
	2460379.8189	0.0002	0.5	0.0015
J05	2460285.6782	0.0003	0	0.0000
	2460285.7825	0.0003	0.5	-0.0004
	2460285.8870	0.0004	1	-0.0006
	2460285.9924	0.0003	1.5	0.0001
J07	2460336.7690	0.0003	0	0.0000
	2460336.8830	0.0003	0.5	0.0007
J08	2460339.7910	0.0004	0	0.0000
	2460339.9140	0.0003	0.5	-0.0004
LO Psc	2460231.3385	0.0006	0	0.0000
	2460231.5121	0.0007	0.5	0.0008
	2460241.3594	0.0005	29	-0.0006
	2460241.5319	0.0004	29.5	-0.0008
N49	2460335.8707	0.0003	0	0.0000
	2460335.9982	0.0004	0.5	0.0054
N65	2460270.8202	0.0002	0	0.0000
	2460270.9522	0.0002	0.5	-0.0001
OT UMa	2459971.4650	0.0005	0	0.0000
	2459986.3209	0.0008	47	0.0008
PU Vir	2460377.7636	0.0002	0	0.0000
	2460377.8957	0.0002	0.5	0.0040
V0801 And	2460264.2968	0.0005	0	0.0000
	2460264.4317	0.0004	0.5	0.0015
	2460266.2979	0.0005	7.5	0.0011

Table 6. The O-C fitting coefficients and mass transfer rate.

System	ΔT_0 ($\times 10^{-4} d$)	Error	ΔP_0 ($\times 10^{-7} d$)	Error	β ($\times 10^{-7} d\ yr^{-1}$)	Error	dM_1/dt ($\times 10^{-7} M_\odot\ yr^{-1}$)	Error
BE Mus	1.05	2.83	0.32	1.88	0	0	0	0
J05	-1.86	5.85	-4.81	2.75	-1.25	0.88	-3.29	2.30
J07	11.61	31.47	7.36	10.30	2.37	2.20	49.89	46.34
J08	-4.41	6.63	7.12	0.42	0	0	0	0
LO Psc	9.98	2.26	-45.87	1.28	-4.48	0.13	3.05	0.10
N49	-4.35	39.30	-29.69	14.21	-5.51	3.25	342.91	201.89
N65	25.65	3.38	19.91	1.50	0.78	0.16	-0.51	0.10
OT UMa	46.86	1.59	60.42	0.58	0	0	0	0
PU Vir	34.43	56.79	43.03	10.37	2.01	0.92	-31.12	14.23
V0801 And	41.67	2.52	9.97	0.17	0	0	0	0

5. LIGHT CURVE SOLUTIONS

We prepared the data for the light curve analysis process. For this purpose, we used the most recent TESS sector if the TESS data was available for each system. Otherwise, the V filter data was used for the process (Table 4). Light curve analyses of the target binary systems were carried out using the PHOEBE Python code version 2.4.9 and the MCMC approach (Prša et al. 2016, Conroy et al. 2020). According to the classification of the target systems in the catalogs, we used contact mode for light curve analysis, considering that contact binary systems are indicated by the short orbital period and shape of light curves. We also obtained the systems' phase shift using reference ephemeris.

It was assumed that $g_1 = g_2 = 0.32$ (Lucy 1967) and $A_1 = A_2 = 0.5$ (Ruciński 1969) were the gravity-darkening coefficients and the bolometric albedo, respectively. The stellar atmosphere was modeled using the Castelli & Kurucz (2004) method, and the limb-darkening coefficients were employed as free parameters in PHOEBE.

We obtained the input effective temperature (T) to start the analysis process from the Gaia DR3 results. Gaia DR3 did not report temperature for the LO Psc system, and the result of TESS was used. This temperature was set according to the depth of minima on the hotter star of the system. We estimated the effective temperature of the other component by using the difference in the depth of the primary and secondary minima.

We used q-search in the photometric observations to carry out the standards required to estimate the mass ratio (q) of the systems (Terrell & Wilson 2005). There are specific values of inclination (i) and fillout factor (f) for each obtained mass ratio value.

The well-known O'Connell effect (O'Connell 1951) is indicated by the asymmetry in the brightness of maxima in the light curve of eclipsing binary stars. The presence of magnetic activity on the star's surface could be a possible explanation for this phenomenon, which causes the existence of a starspot. Due to the apparent magnitude difference in the maxima, eight target systems needed a starspot in the light curve solutions (Table 7). Colatitude (Col.°), longitude (Long.°), angular radius (Radius°), and the ratio of temperature (T_{spot}/T_{star}) are the characteristics that are commonly identified for a starspot (Table 7).

Considering that the presence of a starspot on the systems may affect the results of the initial values, we repeated the q-search process to be sure. Then, we tried to determine the acceptable theoretical fit on the observation data by using the initial values obtained for $T_{1,2}$, q, f, and i. Additionally, we employed PHOEBE's optimization tool to improve the output of light curve solutions and yield the intended results.

The MCMC approach based on the emcee package (Foreman-Mackey et al. 2013) was used to obtain the final values of the parameters and their uncertainty. Therefore, six main parameters, including i, q, f, $T_{1,2}$, and l_1, along with four starspot parameters (coordinates, radius, and T_{spot}/T_{star}), if any, were considered for the MCMC modeling process. We set the appropriate Gaussian distribution to cover the entire observational light curve. We employed 96 walkers and 5000 iterations for ten binary systems. Through the process of light curve analysis, l_3 was not detected in the target systems.

Table 7 presents the outcomes of the light curve solutions, and Figure 2 displays the observed and final synthetic light curves of the binary systems. Figure 3 shows the corner plot of the N65 system as a sample that was determined by MCMC modeling. The rest of the corner plots of other target systems are available in the online version of this study. The three dimensions (3D) of the binary systems and the starspots on the stars are displayed in Figure 4. It should be mentioned the effective temperature variations on the surface of the stars are represented by the color in Figure 4.

6. FUNDAMENTAL PARAMETERS

The accuracy of absolute parameter estimations is significant for investigating the evolution of contact systems and trying to solve some challenges. So, there are various methods used to calculate the absolute parameters of the contact binary systems. Using the Gaia DR3 parallax is one of the methods used for this estimation when photometric data is available (Li et al. 2021). This method of estimation was described in detail in the Poro et al. (2024c) study. The Gaia DR3 parallax method can be accurate and even reveal some flaws in the light curve solution, especially when the reported parallax is accurate enough. However, there are two other influential parameters in this method of estimating absolute parameters, including the interstellar extinction A_V and V_{max}. The first parameter to be calculated is the M_V of the system for which parameters V_{max}, d(pc), and A_V are used, which affects the accuracy of further calculations. The accuracy of V_{max} is related to the observations' accuracy, and this parameter should be determined from the maxima on which the starspot is not placed. Additionally, a large value for the A_V parameter makes it hard to expect proper accuracy in estimating absolute parameters using the Gaia DR3 parallax. We calculated A_V from the 3D dust map based on the Gaia distance (Green et al. 2019). Therefore, systems BE Mus, J05, and J07 have inappropriate A_V values (Table 8) to use Gaia DR3 parallax to this estimation. Therefore, it was inevitable to use another method dependent on the empirical parameter relationship to estimate the absolute parameters of the target systems.

Table 7. Light curve solutions of the target binary systems.

Parameter	BE Mus	J05	J07	J08	LO Psc	N49	N65	OT UMa	PU Vir	V0801 And
T_1 (K)	$5939^{+(11)}_{-(9)}$	$4139^{+(11)}_{-(11)}$	$4702^{+(6)}_{-(7)}$	$4862^{+(7)}_{-(6)}$	$5368^{+(8)}_{-(8)}$	$4177^{+(8)}_{-(11)}$	$5195^{+(7)}_{-(9)}$	$5906^{+(6)}_{-(7)}$	$5125^{+(11)}_{-(12)}$	$4514^{+(7)}_{-(7)}$
T_2 (K)	$5916^{+(10)}_{-(12)}$	$4162^{+(11)}_{-(9)}$	$4572^{+(6)}_{-(5)}$	$4989^{+(7)}_{-(7)}$	$5140^{+(10)}_{-(8)}$	$4432^{+(7)}_{-(7)}$	$5259^{+(7)}_{-(7)}$	$5454^{+(11)}_{-(8)}$	$4809^{+(10)}_{-(13)}$	$4726^{+(6)}_{-(7)}$
$q = M2/M1$	$0.976^{+(13)}_{-(9)}$	$0.693^{+(17)}_{-(14)}$	$0.959^{+(17)}_{-(13)}$	$1.364^{+(16)}_{-(11)}$	$2.394^{+(13)}_{-(10)}$	$1.009^{+(12)}_{-(15)}$	$3.019^{+(23)}_{-(27)}$	$1.600^{+(12)}_{-(15)}$	$1.057^{+(25)}_{-(24)}$	$0.628^{+(6)}_{-(5)}$
i°	$61.40^{+(4)}_{-(4)}$	$59.24^{+(4)}_{-(6)}$	$68.73^{+(5)}_{-(4)}$	$64.56^{+(4)}_{-(4)}$	$89.80^{+(7)}_{-(7)}$	$52.53^{+(25)}_{-(4)}$	$76.50^{+(4)}_{-(4)}$	$62.16^{+(4)}_{-(3)}$	$41.64^{+(8)}_{-(6)}$	$74.52^{+(3)}_{-(5)}$
f	$0.100^{+(5)}_{-(3)}$	$0.191^{+(3)}_{-(5)}$	$0.120^{+(3)}_{-(2)}$	$0.034^{+(4)}_{-(3)}$	$0.357^{+(4)}_{-(3)}$	$0.047^{+(3)}_{-(3)}$	$0.125^{+(4)}_{-(4)}$	$0.061^{+(3)}_{-(3)}$	$0.119^{+(4)}_{-(4)}$	$0.105^{+(4)}_{-(3)}$
$\Omega_1 = \Omega_2$	3.658(7)	3.155(5)	3.620(4)	4.302(3)	5.583(5)	3.739(6)	6.564(8)	4.639(5)	3.777(6)	3.076(5)
l_1/l_{tot}	$0.509^{+(1)}_{-(1)}$	$0.573^{+(1)}_{-(1)}$	$0.557^{+(1)}_{-(1)}$	$0.391^{+(1)}_{-(1)}$	$0.356^{+(1)}_{-(1)}$	$0.436^{+(1)}_{-(1)}$	$0.257^{+(1)}_{-(1)}$	$0.463^{+(1)}_{-(1)}$	$0.584^{+(1)}_{-(1)}$	$0.553^{+(1)}_{-(1)}$
l_2/l_{tot}	0.491(1)	0.427(1)	0.443(1)	0.609(1)	0.644(1)	0.564(1)	0.743(1)	0.537(1)	0.416(1)	0.447(1)
$r_{(mean)1}$	0.391(3)	0.428(4)	0.395(3)	0.356(3)	0.332(3)	0.384(4)	0.296(2)	0.344(3)	0.386(4)	0.430(4)
$r_{(mean)2}$	0.387(3)	0.364(3)	0.388(3)	0.410(4)	0.482(5)	0.385(3)	0.486(5)	0.427(4)	0.396(4)	0.348(3)
Phase Shift	0.005(1)	0.000(1)	-0.004(1)	0.000(1)	0.017(1)	0.051(1)	-0.019(1)	0.013(1)	0.000(1)	0.013(1)
Starspot:										
Col.(deg.)	$112.7^{+(1.1)}_{-(1.3)}$	$123.1^{+(1.6)}_{-(1.8)}$	$107.3^{+(1.1)}_{-(0.9)}$	$106.6^{+(1.5)}_{-(1.1)}$		$121.9^{+(7)}_{-(9)}$	$93.0^{+(1.2)}_{-(1.2)}$		$103.5^{+(1.2)}_{-(1.3)}$	$105.5^{+(1.5)}_{-(8)}$
Long.(deg.)	$309.4^{+(1)}_{-(1)}$	$66.5^{+(1.4)}_{-(1.6)}$	$320.5^{+(1.1)}_{-(0.9)}$	$20.5^{+(1.2)}_{-(1.2)}$		$46.3^{+(1.1)}_{-(1.1)}$	$43.6^{+(1.0)}_{-(9)}$		$302.4^{+(2.1)}_{-(2.1)}$	$256.6^{+(7)}_{-(9)}$
Radius(deg.)	$17.2^{+(2)}_{-(2)}$	$14.8^{+(3)}_{-(3)}$	$24.1^{+(2)}_{-(2)}$	$13.9^{+(3)}_{-(3)}$		$12.2^{+(2)}_{-(2)}$	$12.1^{+(2)}_{-(2)}$		$18.4^{+(3)}_{-(2)}$	$23.1^{+(1)}_{-(2)}$
T_{spot}/T_{star}	$0.923^{+(3)}_{-(4)}$	$0.873^{+(4)}_{-(5)}$	$0.881^{+(3)}_{-(4)}$	$0.950^{+(2)}_{-(2)}$		$0.940^{+(5)}_{-(4)}$	$0.868^{+(4)}_{-(5)}$		$0.880^{+(4)}_{-(5)}$	$0.777^{+(5)}_{-(5)}$
Star	Secondary	Secondary	Secondary	Secondary		Secondary	Secondary		Secondary	Secondary

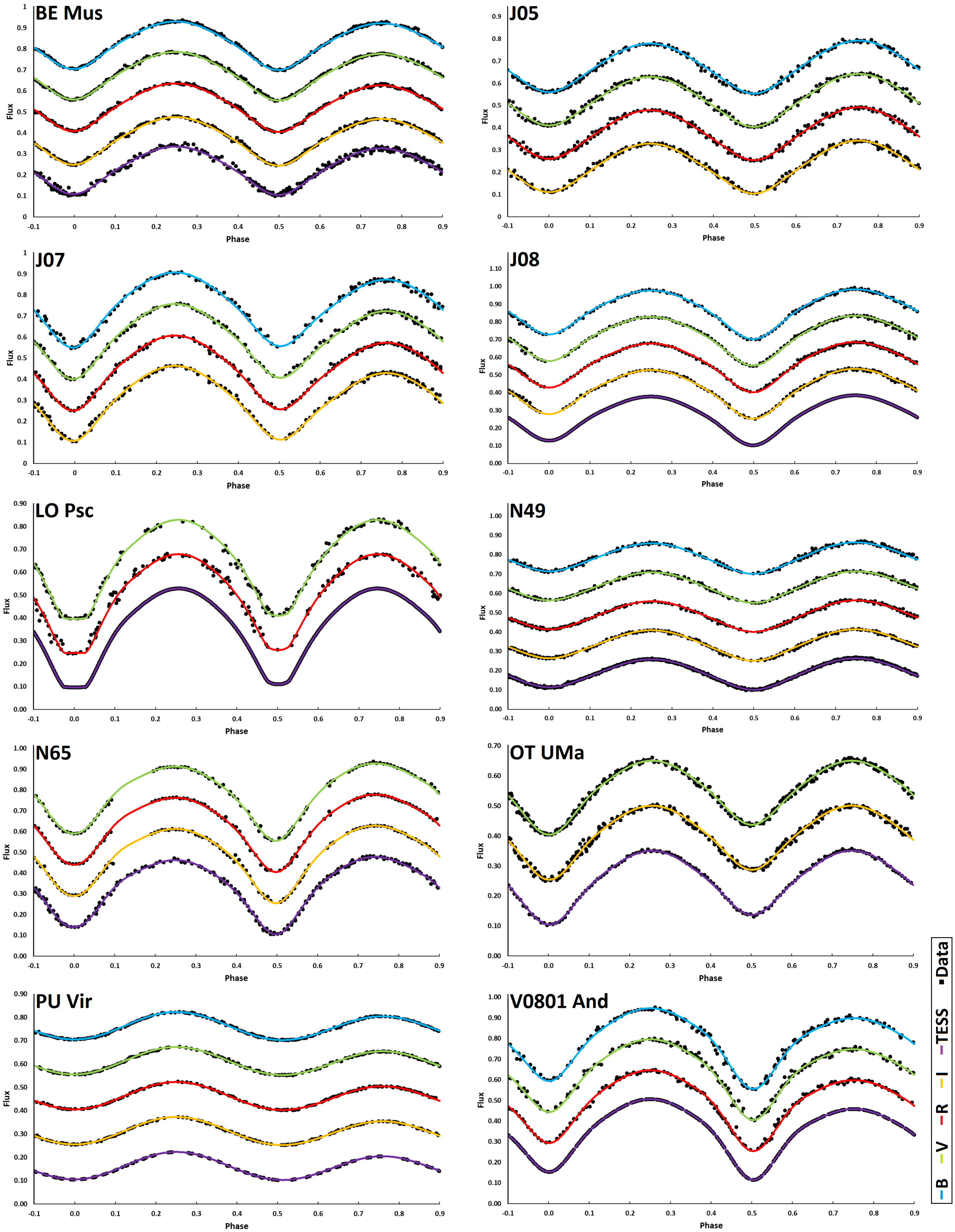
BE Mus
J05
J07
J08
LO Psc
N49
N65
OT UMa
PU Vir
V0801 And
Flux
Phase
B
V
R
I
TESS
Data

Figure 2. .

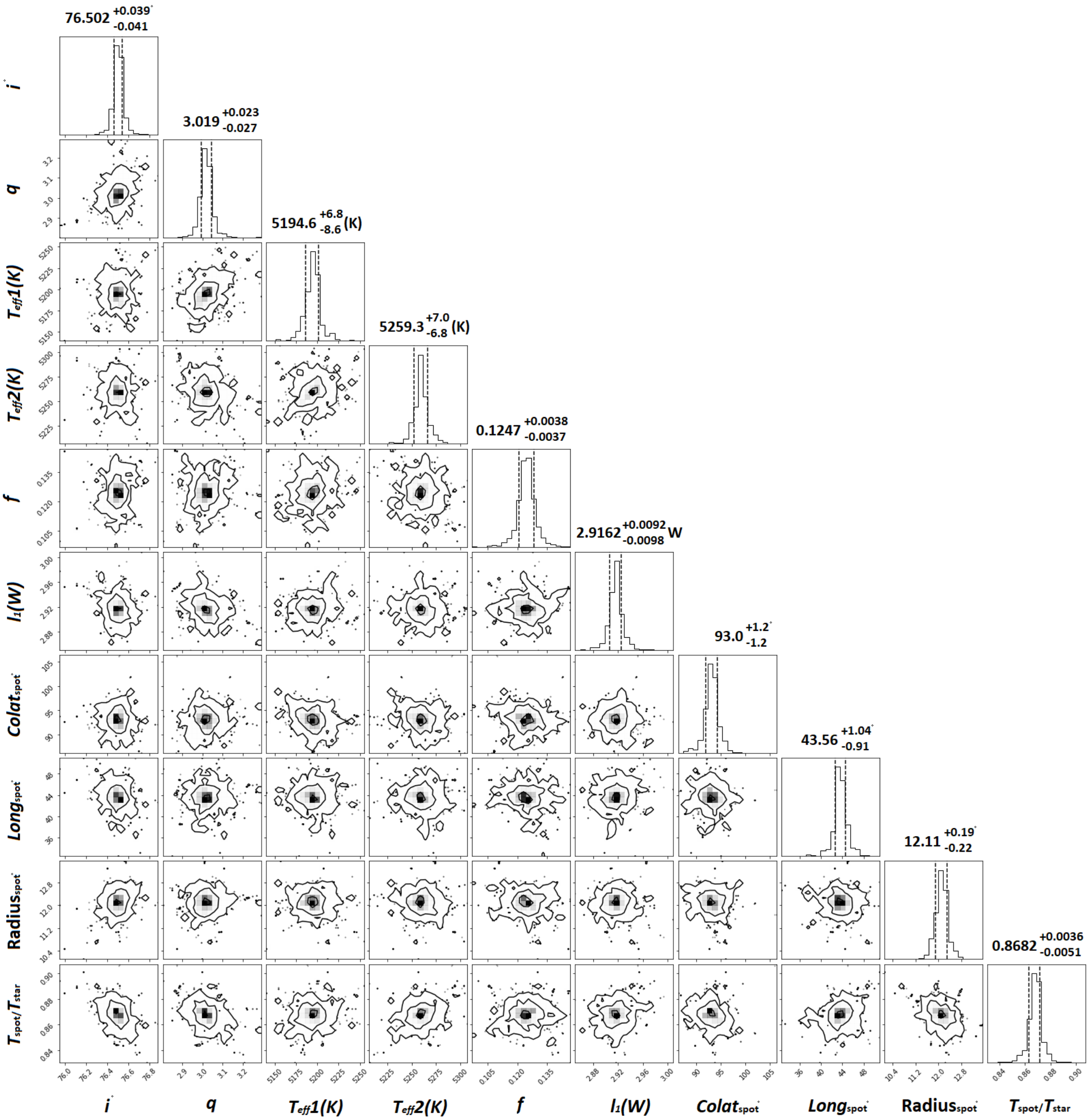

Figure 3. The corner plots of the N65 system were determined by MCMC modeling. Corner plots for other target systems are available in the online version of this study.

Poro et al. (2024a) updated the orbital period and semi-major axis ($P-a$) empirical relationship using 414 contact binary systems with orbital periods less than 0.7 days (Equation 3).

$$a = (0.372^{+0.113}_{-0.114}) + (5.914^{+0.272}_{-0.298}) \times P \tag{3}$$

The estimation process for the absolute parameters started with Equation 3. Therefore, each target system's orbital period was used to obtain the value of $a(R_\odot)$. We used the mass ratio from the light curve solutions and Kepler's

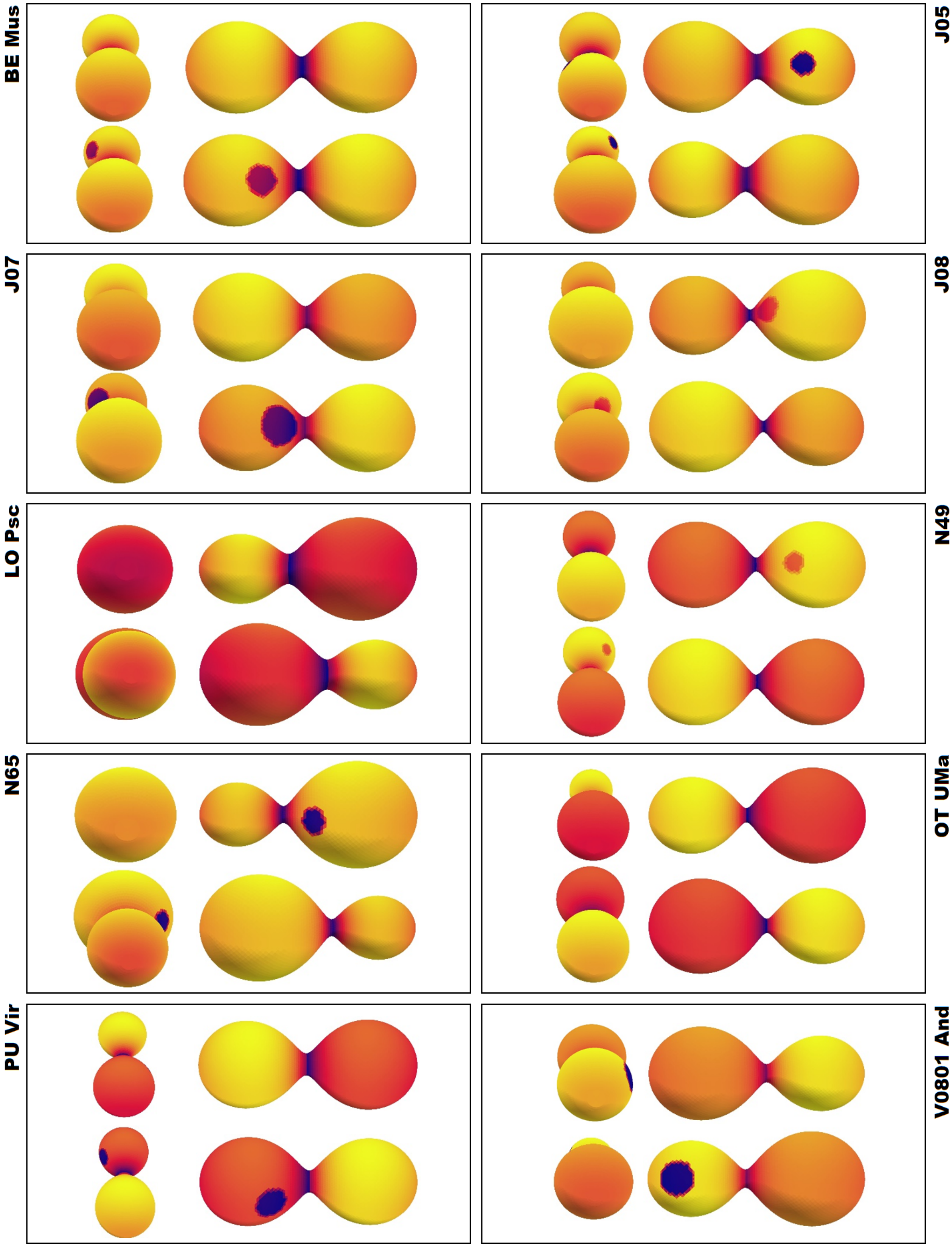

Figure 4. 3D view of stars in the binary systems.

Table 8. Estimated absolute parameters of the systems.

Parameter	BE Mus	J05	J07	J08	LO Psc	N49	N65	OT UMa	PU Vir	V0801 And
$M_1(M_\odot)$	0.79(23)	0.76(27)	0.67(23)	0.57(19)	0.47(13)	0.67(22)	0.35(11)	0.58(17)	0.67(22)	0.86(28)
$M_2(M_\odot)$	0.77(24)	0.52(20)	0.64(24)	0.78(27)	1.12(33)	0.68(24)	1.05(35)	0.93(29)	0.71(25)	0.54(18)
$R_1(R_\odot)$	0.92(9)	0.69(8)	0.68(8)	0.65(7)	0.80(8)	0.70(8)	0.57(6)	0.77(8)	0.73(8)	0.84(9)
$R_2(R_\odot)$	0.92(9)	0.59(7)	0.66(7)	0.75(8)	1.16(12)	0.70(8)	0.94(10)	0.96(10)	0.75(8)	0.68(7)
$L_1(L_\odot)$	0.96(20)	0.13(3)	0.20(5)	0.21(5)	0.48(10)	0.13(3)	0.22(5)	0.65(14)	0.33(8)	0.26(6)
$L_2(L_\odot)$	0.92(20)	0.09(2)	0.17(4)	0.32(8)	0.85(18)	0.17(4)	0.61(14)	0.73(16)	0.27(7)	0.21(5)
$M_{bol1}(mag.)$	4.78(21)	6.98(25)	6.47(24)	6.40(23)	5.52(21)	6.92(24)	6.40(22)	5.19(21)	5.93(24)	6.18(23)
$M_{bol2}(mag.)$	4.82(21)	7.31(25)	6.63(24)	5.98(23)	4.90(21)	6.65(23)	5.27(23)	5.07(22)	6.15(24)	6.44(23)
$M_{V1}(mag.)$	4.83(21)	7.92(24)	6.93(23)	6.78(23)	5.70(21)	7.81(23)	6.63(22)	5.25(21)	6.19(23)	6.77(22)
$M_{V2}(mag.)$	4.87(21)	8.22(24)	7.18(23)	6.30(23)	5.15(21)	7.31(23)	5.47(23)	5.22(21)	6.56(23)	6.89(22)
$log(g)_1(cgs)$	4.40(3)	4.64(4)	4.60(4)	4.57(3)	4.30(3)	4.58(3)	4.46(3)	4.43(3)	4.54(3)	4.53(3)
$log(g)_2(cgs)$	4.40(4)	4.62(5)	4.60(4)	4.58(4)	4.35(3)	4.58(4)	4.51(4)	4.44(3)	4.54(4)	4.51(4)
$a(R_\odot)$	2.36(21)	1.61(17)	1.71(18)	1.83(18)	2.42(21)	1.82(18)	1.93(19)	2.24(20)	1.89(19)	1.95(19)
BC_1	-0.054(2)	-0.938(13)	-0.464(4)	-0.374(3)	-0.173(2)	-0.894(11)	-0.229(3)	-0.059(1)	-0.255(5)	-0.589(5)
BC_2	-0.057(1)	-0.911(12)	-0.548(4)	-0.313(3)	-0.250(4)	-0.652(6)	-0.207(2)	-0.149(3)	-0.402(6)	-0.449(4)
A_V	0.405(2)	0.731(2)	0.248(1)	0.085(4)	0.078(1)	0.037(1)	0.209(1)	0.073(1)	0.067(1)	0.118(1)

well-known third law equation to estimate the mass and uncertainty of each star. The radius (R) of each companion was calculated using $r_{mean1,2}$ from the light curve solutions and the equation $R = a \times r$. The effective temperature and radius of each star make it possible to calculate the luminosity of the components. The luminosity was employed to determine the absolute bolometric magnitude (M_{bol}) by utilizing the relationship between the stellar parameters. The Sun's absolute bolometric magnitude is considered to be 4.73^{mag} based on the Torres (2010) study. The absolute magnitude (M_V) value of the stars in the target systems was also calculated using the Bolometric Correction (BC) from the Flower (1996) study and the equation $M_V = M_{bol} - BC$. Then, we estimated the surface gravity (g) of the stars on a logarithmic scale using M and R parameters. The results of estimating ten binary systems' absolute parameters are presented in Table 8.

7. DISCUSSION AND CONCLUSION

We presented an orbital period variation, the first light curve analysis, and absolute parameters estimations of ten contact binary systems. Observations of these binary systems were performed at four observatories in the northern and southern hemispheres with multiband standard filters. Based on the analysis and results, the following are presented as discussions and conclusions:

A) The long-term increase in the orbital period is usually caused by mass transfer from the less massive component to the more massive component, while the continuous orbital period decrease generally results from mass transfer from the more massive component to the less massive one or from AML or their combination. Using the following equation from the Kwee (1958) study,

$$\frac{\dot{P}}{P} = -3\dot{M}(\frac{1}{M_1} - \frac{1}{M_2}), \tag{4}$$

We calculated the mass transfer rate for the target systems as shown in 6. For J05, LO Psc, and N49, their orbital periods are continuously decreasing, and the more massive component is losing mass. We use the equation $\tau_{th} = \frac{GM_1^2}{R_1 L_1}$ to calculate the thermal timescale for them, and $\tau_{th} = 2.02 \times 10^8 yr$ for J05, $\tau_{th} = 4.00 \times 10^7 yr$ for LO Psc, and $\tau_{th} = 1.22 \times 10^8 yr$ for N49 are obtained. The thermal mass transfer rate was calculated to be $M_h/\tau_{th} = 3.75 \times 10^{-9} M\odot$ yr^{-1} for J05, $M_h/\tau_{th} = 2.80 \times 10^{-8} M\odot\ yr^{-1}$ for LO Psc, and $M_h/\tau_{th} = 5.57 \times 10^{-9} M\odot\ yr^{-1}$ for N49 (M_h means the mass of the more massive component). Since these three values differ significantly from those calculated in Table

6, it implies that the reduction in orbital period is caused by AML rather than mass transfer.

B) The stars in the target systems have a temperature range of 4100 K to 5900 K. The BE Mus and J05 systems are associated with the lowest temperature differential between two companion stars, whereas OT UMa has the highest temperature differential (Table 10). Based on the Cox (2000) and Eker et al. (2018) studies, the effective temperature of the stars indicates that they are in the G and K spectral categories (Table 10).

C) This study has found that system LO Psc is a total eclipse, while other target systems are partial eclipse binary systems. Theoretically, when a total eclipse occurs in the system, parameters such as inclination and fillout factor have less influence on the q-search process to obtain the mass ratio. Therefore, if a proper light curve analysis is performed, it can be expected that the mass ratio of total eclipse binary systems will be acceptable. Can such accuracy be obtained with partial eclipse systems? Some studies statistically compared the mass ratio derived from spectroscopic data (q_{sp}) with photometry data (q_{ph}) and found that total eclipse systems' trend was closer to the q_{sp} results than partial eclipses (e.g., Hambálek & Pribulla 2013 Li et al. 2021, Kouzuma 2023). So, there is a general view that photometric mass ratios cannot be accurately determined for systems that have partial eclipses. It seems that this view can be critically examined.

We produced a comparison plot of q_{sp} and q_{ph} by employing 100 contact binary systems from a sample used in the Li et al. (2021) study and adding 13 additional systems from literature (Table 9). In Figure 5, the systems with blue (total eclipse) and green (partial eclipse) colors represent the system used by Li et al. (2021), and the systems with red colors are the systems added in this study. We used the $i > arccos|(r_1 - r_2)/a|$ relationship to determine each system type, and all 13 were partial eclipses (Sun et al. 2020). We plotted a linear fit on total eclipsed systems with uncertainty that was very close to a one-to-one linear fit (Figure 5). As it is clear in Figure 5, the systems with partial eclipse that we added show a behavior similar to the total eclipse systems. Therefore, there are always systems that significantly change the experimental result. Currently, the number of systems that have both q_{sp} and q_{ph} is very limited. So, it is hard to draw firm conclusions for partial eclipse systems with this number of sample systems for investigations. In fact, the biggest obstacle to having a definitive statement about total and partial eclipse systems is a suitable and much larger sample. It is also challenging to select spectroscopic and photometric studies for the sample; ideally, in a study including spectroscopy, both q_{sp} and q_{ph} should be determined.

The Li et al. (2021) study used 101 contact systems for their sample, but we used 100 of them. The system that has changed is related to LS Del (Table 9). The case of LS Del as a partial eclipse system shows that light curve analysis with photometric data can provide more suitable results. Most of the selected systems in Table 9 have been selected from studies whose light curve analysis has been done in some way using the MCMC method or MC simulation, and they showed very good compatibility with the linear fit in Figure 5. There are some important factors to consider when determining the mass ratio using spectroscopic data, so these observations need the necessary accuracy, good resolution of the spectroscopic instrument, telescope aperture, and observation periods. For example, the KR Com system has a $q_{sp} = 0.091(2)$ from the Rucinski et al. (2002) study, which is a close value to the photometric study selected in Table 9.

On the other hand, in recent years, the use of the MCMC method to obtain parameters and their uncertainty has become much more prominent. In this study, we used the same method for ten contact systems. If there is an error in the initial q-search, MCMC will correct it according to other parameters, and if the q-search is suitable, it will present value more accurately along with uncertainty. However, using the MCMC method has challenges; MCMC is highly dependent on distribution, which should include the entire light curve, and the error bar of the observational data should be reasonable. Therefore, using the results of photometric studies that obtained the mass ratio with MCMC can be more suitable for a sample.

D) Kouzuma (2023) suggested a new method to estimate the photometric mass ratio of overcontact binaries using the light curve's derivatives. This method could be different since iterative methods are usually used to estimate the photometric mass ratio or the relationships between the parameters are considered. Through a sample comparison, Kouzuma (2023) found that around 67% of the samples agreed with their spectroscopic mass ratios within the estimated uncertainties and that the errors for 95% of the samples were within ± 0.1.

The discussed method is based on derivation at different orders of the photometric light curve. The Kouzuma (2023) study used 117,600 synthetic light curves as a sample to reach the new method. There are three conditions to use this

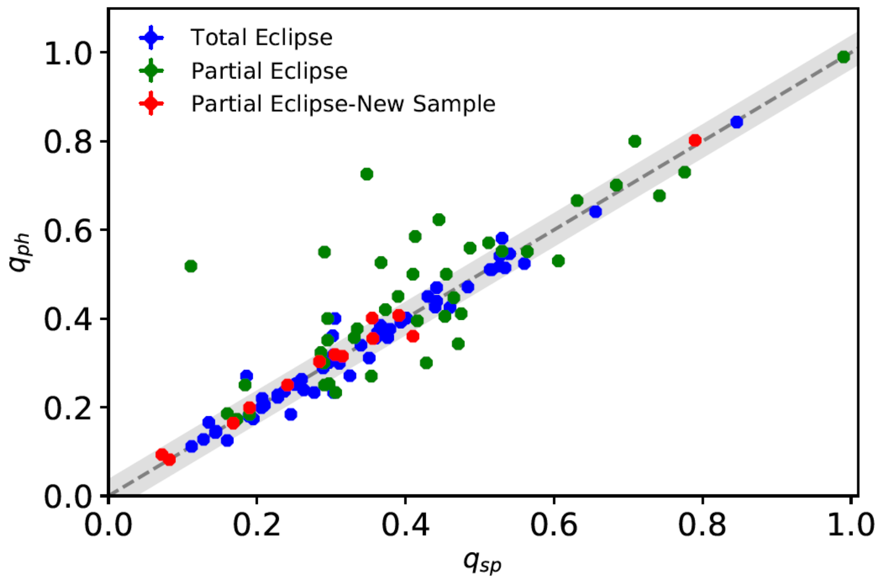

Figure 5. Comparing mass ratio results utilizing spectroscopic (q_{sp}) and photometric (q_{ph}) data for available samples.

method, the most important of which is the existence of maxima and minima in the second and third-order derivations in the desired places. After derivation of the third order and based on the measurement between the minima and maxima that exist and also the orbital period of the system, a parameter named W is measured. The Kouzuma (2023) investigation revealed a strong relationship between W and q.

We attempted to use the Kouzuma (2023) method to estimate the mass ratio for our systems and compared the results with the findings from MCMC and light curve analysis. We thank Shinjirou Kouzuma, who gave us the possibility to use the code for this method. Therefore, it was possible to use this method for five target systems, including J08, LO Psc, N65, OT UMa, and V0801 And. The method is not applicable to the other five systems since there was no appearance of a double peak in the second derivative of the light curve. Considering that the mass ratio estimated by the Kouzuma (2023) method is based on $1/q$, the results are shown in Table 10 for five target systems. Figure 6 also shows the process of estimation for the V0801 And system. The difference between the mass ratio obtained in the study and the Kouzuma (2023) method is also shown in Table 10, which shows that all of them are within the uncertainty range of ±0.1.

Using light curve derivatives to estimate the photometric mass ratio is a different method and can be effective. We have conducted a review of this new method based on the published study (Kouzuma 2023): 1. In the study of the method, there is no mention of the effect of the starspot in the process of estimating the mass ratio. Therefore, we estimated the mass ratio of the five systems in this study with and without starspot on the light curves. We repeated the same experiment with 21 other contact systems from the accessible data of the Rahimi et al. (2021), Poro et al. (2022b), Poro et al. (2024a), and Paki & Poro (2024) studies. The outcomes revealed a change of less than 2% in each instance. Therefore, it can be concluded that the presence of a starspot in the light curve does not interfere with estimating the mass ratio by this method. 2. we used ground-based and TESS data with different filters for another examination. The quality of all used data was acceptable. It was found that the method cannot estimate the mass ratio in cases where the number of data points is small. Also, in most cases, for light curves with a small amount of scatter, the method cannot estimate the mass ratio for ground-based or TESS data. In the same case, when using TESS data that was extracted one day, the result will be appropriate. Therefore, this method is highly sensitive to data dispersion. Our suggestion is that to estimate the mass ratio with this method, it is better to find the best fit with the software and codes and use it for the input data. 3. Apart from the three conditions mentioned in the study, this method has limitations that make it unsuitable for some contact systems. It seems that this method is more suitable for total or close to total eclipse systems. However, it is a suitable and acceptable accurate method for the initial estimation of the mass ratio, and then it is necessary to use methods such as MCMC to improve its accuracy along with other parameters.

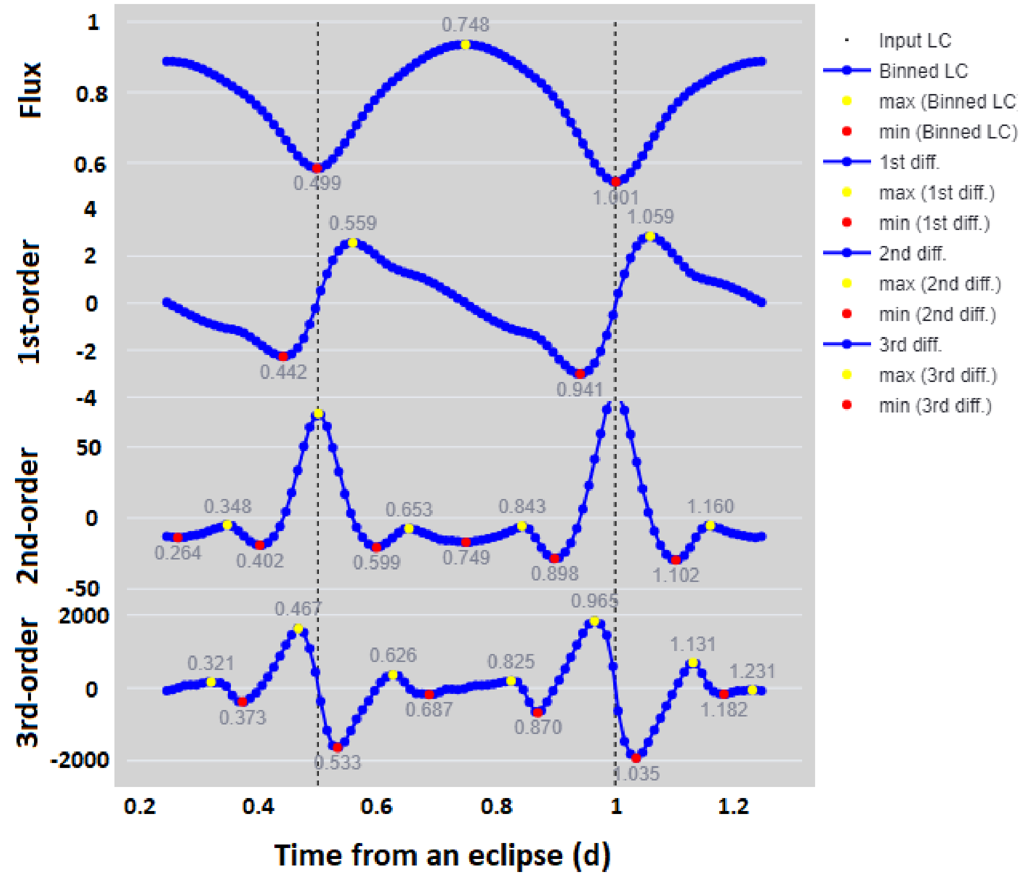

Figure 6. A photometric light curve of V0801 And, and first to third derivatives (top to bottom panels, respectively) as an example of a process for systems. The units of the panels on the vertical axis from top to bottom are W m^{-2}, 10 W m^{-2} day^{-1}, 10^2 W m^{-2} day^{-2}, and 10^4 W m^{-2} day^{-3}, respectively.

E) Figure 7 displays the 18 parameters' two-dimensional relationships and the positions of the ten studied systems. Based on the light curve analysis and the estimation of absolute parameters, we presented the evolution state of the ten systems on the Hertzsprung-Russell (HR), Mass-Luminosity ($M - L$), and Mass-Radius ($M - R$) diagrams (Figure 7a,b,d,e,g,h). The positions of the stars were displayed in each of these diagrams relative to the Zero-Age Main Sequence (ZAMS) and Terminal-Age Main Sequence (TAMS) lines. The ZAMS and TAMS lines are from the Girardi et al. 2000 study.

The Poro et al. (2024d) study used 428 contact binary systems to present the $T_h - M_m$ theoretical fit. The more massive star was identified as M_m. Based on the star's mass determined by estimating the absolute parameters and the effective temperature obtained from the light curve analysis, we placed the star's position on the $T_h - M_m$ diagram (Figure 7c). There is good agreement between the position of the primary star and this theoretical fit and uncertainty. The gray points in Figure 7c are the samples used in the Poro et al. (2024d) study, which were compared with the studied systems.

Furthermore, we displayed the star positions on the $log(g)_1 - logT_1$ diagram (7f), which was derived from the Yıldız (2015) study. In the diagram, the stars are positioned between ZAMS and TAMS, with only LO Psc close and above the TAMS line.

The orbital angular momentum of each system was estimated using the Eker et al. (2006) study (Equation 5).

$$J_0 = \frac{q}{(1+q)^2} \sqrt[3]{\frac{G^2}{2\pi} M^5 P} \tag{5}$$

Table 9. Contact binary systems with spectroscopic and photometric observations. Orbital periods are from the VSX database.

System	P(day)	q_{sp}	q_{ph}	i°	References
YY Crb	0.376565	0.241	0.25	81.5	Soomandar & Poro (2024), Essam et al. (2010)
V870 Ara	0.399773	0.082	0.082	73.6	Poro et al. (2021), Szalai et al. (2007)
DY Cet	0.440790	0.356	0.355	85.6	Pribulla et al. (2009), Yıldırım (2022)
LO And	0.3804418885	0.305	0.319	80.1	Huang et al. (2021), Nelson & Robb (2015)
KR Com	0.40797003	0.072	0.093	52.1	Gazeas et al. (2021), Mitnyan et al. (2020)
V1073 Cyg	0.785850	0.284	0.303	68.4	Tian et al. (2018), Mitnyan et al. (2020)
V2150 Cyg	0.5918609	0.79	0.802	43.4	Kreiner et al. (2003), Mitnyan et al. (2020)
LS Del	0.363842	0.391	0.407	47.8	Poro et al. (2024e), Mitnyan et al. (2020)
V972 Her	0.443094	0.168	0.164	40.1	Selam et al. (2018), Mitnyan et al. (2020)
EX Leo	0.4086041	0.19	0.199	60.8	Zola et al. (2010), Mitnyan et al. (2020)
V351 Peg	0.593297	0.41	0.36	63.0	Albayrak et al. (2005), Mitnyan et al. (2020)
V357 Peg	0.5784511	0.355	0.401	73.2	Deb & Singh (2011), Mitnyan et al. (2020)
EE Cet	0.379925	0.315	0.315	78.5	Djurašević et al. (2006), Gazeas et al. (2021)

where q is the mass ratio, M is the total mass of the system, P is the orbital period, and G is the gravitational constant. Table 10 contains a list of the systems' $log(J_0)$ computation results. According to the values of M_{tot} and $log(J_0)$, and the theoretical fit of Eker et al. (2006), our systems are in the region of contact binary systems (Figure 7i).

The stars' positions in the theoretical relationship from the Poro et al. (2024b) study were also examined. The positions of the stars are in good agreement with the $P - L_{1,2}$ relationships, as Figure 7j,k illustrates. Also in these diagrams, we displayed a sample of 118 contact binary systems from the Poro et al. (2024b) study that had an orbital period shorter than 0.6 days and absolute parameters were estimated based on the Gaia DR3 parallax.

The relationship between the orbital period and mass ($P - M$) of the stars in contact systems has been the subject of numerous statistical investigations (Qian 2003, Kouzuma 2018, Latković et al. 2021, Poro et al. 2022a). According to the available samples, there is not a very strong relationship between these two parameters, but there seems to be a definite trend. So we showed the placement of the ten target systems in the latest study on $P - M$ relationships, Poro et al. (2022a). Figure 7m,n,q show relationships with more massive stars (M_m), less massive stars (M_l), and total mass of stars (M_{tot}). In the same study (Poro et al. 2022a), the relationship between P and $log(g)_1$ was also shown in Figure 7r. The location of the stars in the theoretical fits is in good agreement with their trends.

Additionally, we examined our results on the radius ratio and luminosity ratio of the stars with the mass ratio of the systems ($M_2/M_1 - R_2/R_1$ and $M_2/M_1 - L_2/L_1$). These relationships have come from the Poro et al. (2022b) and Poro et al. (2024b) studies, respectively. The positions of the stars in these theoretical fits coincide with their trends. The gray points in the $M_2/M_1 - L_2/L_1$ diagram correspond to the sample of the Poro et al. (2024b) study.

Figure 7p depicts the relationship between the orbital period and the system's absolute magnitude ($P - M_V$). The theoretical fit of this relationship is from the Poro et al. (2024b) study. Equation 6 was utilized to obtain the system's absolute value:

$$M_V = V_{max} - 5log(d) + 5 - A_V \tag{6}$$

where V_{max} is the maximum apparent magnitude of the system based on our observations, d is the star's distance resulting from Gaia DR3 and A_V is the result of the calculations in this study. The calculated M_V values are presented in Table 10. Apart from system J05, nine other systems are within the uncertainty of $P - M_V$ fit. This shows that the high value of A_V can affect the calculations, especially if the Gaia DR3 parallax was used to estimate the absolute parameters.

DATA AVAILABILITY

Ground-based data will be made available on request.

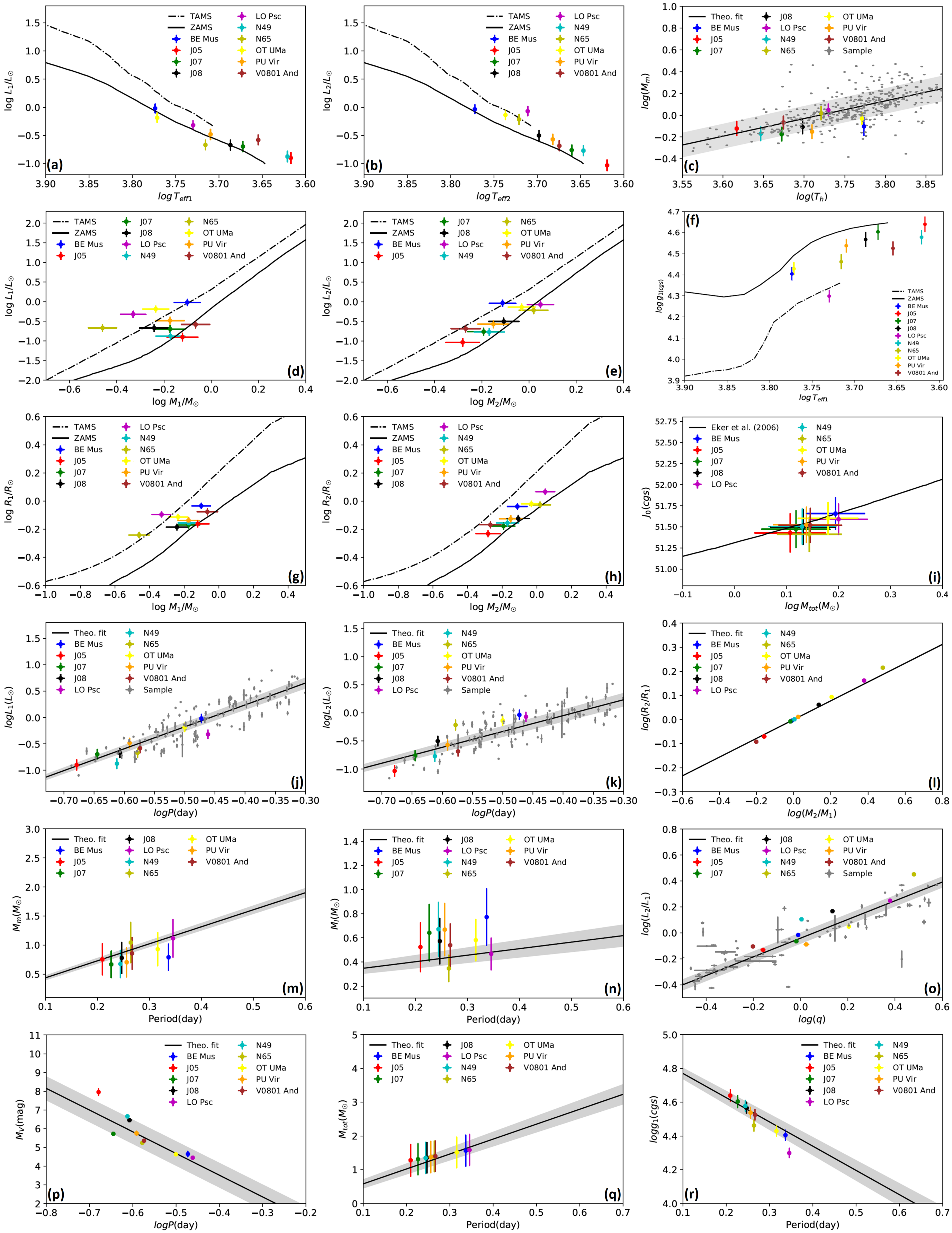

Figure 7. The position of the target systems in different diagrams of the parameter relationships.

Table 10. Values of the temperature difference between companions, calculated mass ratio based on derivations from the light curve and also difference with this study's estimation, total mass, angular orbital momentum, systems' absolute magnitude, spectral category of components, and each system's subtype, respectively.

Parameter	BE Mus	J05	J07	J08	LO Psc	N49	N65	OT UMa	PU Vir	V0801 And
ΔT (K)	23	23	130	127	228	255	64	452	316	212
Sp. category	G1/G1	K5/K5	K3/K4	K2/K1	K0/K1	K5/K5	K0/K0	G1/G8	K1/K2	K4/K5
$1/q^{*}$[a]	-	-	-	0.650	0.384	-	0.422	0.547	-	0.568
$\Delta 1/q$[b]	-	-	-	0.083	0.034	-	0.091	0.078	-	0.060
$M_{tot}(M_{\odot})$	1.56(46)	1.28(47)	1.31(47)	1.35(46)	1.58(46)	1.35(46)	1.39(46)	1.51(46)	1.37(47)	1.40(45)
$log(J_0)$	51.66(19)	51.43(23)	51.47(22)	51.50(21)	51.59(18)	51.50(21)	51.41(20)	51.60(19)	51.52(21)	51.52(20)
$M_V(mag.)$	4.65(15)	7.95(19)	5.73(7)	6.45(6)	4.45(8)	6.66(9)	5.24(7)	4.64(7)	5.75(12)	5.36(8)
System type	A	W	A	W	W	W	W	W	W	W

[a] The obtained values for mass ratio based on the Kouzuma (2023) study method.

[b] The difference in mass ratio obtained by Kouzuma (2023) method and this study's results ($1/q$).

ACKNOWLEDGEMENTS

This manuscript was prepared by the BSN project. We used IRAF, which is distributed by the National Optical Observatories and operated by the Association of Universities for Research in Astronomy, Inc., under a cooperative agreement with the National Science Foundation. We used data from the European Space Agency's mission Gaia[9]. This work includes data from the TESS mission observations. The NASA Explorer Program provides funding for the TESS mission. This paper used some results from the American Association of Variable Star Observers (AAVSO[10]). We appreciate the helpful comments from Ehsan Paki.

ORCID IDS

Atila Poro: 0000-0002-0196-9732
Kai Li: 0000-0003-3590-335X
Angel Castro: 0000-0002-7832-5337
Raul Michel: 0000-0003-1263-808X
Eduardo Fernández Lajús: 0000-0002-9262-4456
Fahri Alicavus: 0000-0002-1972-8400
Jean-François COLIAC: 0000-0003-0354-8568
Yasemin Aladağ: 0000-0002-6107-579X
Ailar Alizadehsabegh: 0000-0001-5768-0340

APPENDIX

The times of minima extracted from space-based data and collected from literature are presented in the appendix tables for ten studied systems. Due to the length of some tables containing space-based minima times, they are available in machine-readable form.

[9] http://www.cosmos.esa.int/gaia

[10] https://www.aavso.org/

Table 1. The BE Mus system's times of minima.

Min.(BJD_{TDB})	Epoch	O-C	Source	Min.(BJD_{TDB})	Epoch	O-C	Source
2457849.9743(9)	-7508	-0.0229	ASAS-SN	2460059.0606(4)	-951.5	-0.0018	TESS
2457850.1414(8)	-7507.5	-0.0243	ASAS-SN	2460059.2255(3)	-951	-0.0054	TESS
2458600.1502(6)	-5281.5	-0.0161	TESS	2460059.3966(4)	-950.5	-0.0028	TESS
2458600.3179(7)	-5281	-0.0169	TESS	2460059.5675(5)	-950	-0.0003	TESS
...	...	...	...	...	...	...	...

Table 2. The J05 system's times of minima.

Min.(BJD_{TDB})	Epoch	O-C	Source
2457724.2720(18)	-12230.5	0.0005	ASAS-SN
2458635.1780(5)	-7881	0.0003	ZTF
2458635.2839(5)	-7880.5	0.0015	ZTF
2459187.1261(7)	-5245.5	0.0014	ZTF
2459187.2315(8)	-5245	0.0021	ZTF

Table 3. The J07 system's times of minima.

Min.(BJD_{TDB})	Epoch	O-C	Source	Min.(BJD_{TDB})	Epoch	O-C	Source
2457031.4468(8)	-14591.5	-0.0162	ASAS-SN	2458625.1538(3)	-7556	-0.0096	ZTF
2457031.5618(12)	-14591	-0.0145	ASAS-SN	2458625.2668(3)	-7555.5	-0.0099	ZTF
2458010.4749(19)	-10269.5	-0.0192	ASAS-SN	2459625.1435(4)	-3141.5	-0.0044	ZTF
2458010.5912(27)	-10269	-0.0162	ASAS-SN	2459625.2570(5)	-3141	-0.0042	ZTF

Table 4. The J08 system's times of minima.

Min.(BJD_{TDB})	Epoch	O-C	Source	Min.(BJD_{TDB})	Epoch	O-C	Source
2457200.0496(8)	-12717.5	-0.0081	ASAS-SN	2459522.4828(1)	-3310.5	-0.0024	TESS
2457200.1716(10)	-12717	-0.0095	ASAS-SN	2459528.5308(1)	-3286	-0.0030	TESS
2458050.0665(8)	-9274.5	-0.0090	ASAS-SN	2459528.6550(2)	-3285.5	-0.0022	TESS
2458050.1889(8)	-9274	-0.0101	ASAS-SN	2454084.6242(15)	-25336.5	-0.0182	SuperWASP
...	...	...	...	...	...	...	...

Table 5. The N49 system's times of minima.

Min.(BJD_{TDB})	Epoch	O-C	Source	Min.(BJD_{TDB})	Epoch	O-C	Source
"2457375.0222(7)	-12126.5	0.0087	ASAS-SN	2458894.7032(1)	-5902.5	0.0117	TESS
2457375.1419(14)	-12126	0.0063	ASAS-SN	2459615.0992(1)	-2952	0.0012	TESS
"2458873.5838(1)	-5989	0.0125	TESS	2459615.2280(1)	-2951.5	0.0080	TESS
"2458873.7052(1)	-5988.5	0.0118	TESS	2459619.1346(1)	-2935.5	0.0079	TESS
"2458880.0534(1)	-5962.5	0.0118	TESS	2459619.2504(1)	-2935	0.0017	TESS
"2458880.1761(1)	-5962	0.0124	TESS	2459630.1221(1)	-2890.5	0.0081	TESS
"2458888.1109(1)	-5929.5	0.0118	TESS	2459630.2372(1)	-2890	0.0011	TESS
"2458888.2339(1)	-5929	0.0127	TESS	2459634.1439(1)	-2874	0.0012	TESS
"2458894.5822(1)	-5903	0.0128	TESS	2459634.2727(1)	-2873.5	0.0079	TESS

Table 6. The LO Psc's times of minima.

Min.(BJD_{TDB})	Epoch	O-C	Source	Min.(BJD_{TDB})	Epoch	O-C	Source
2453202.6855(4)	-20339.5	0.0070	SuperWASP	2459857.6135(2)	-1081.5	0.0058	TESS
2453206.6597(4)	-20328	0.0072	SuperWASP	2459857.7864(2)	-1081	0.0058	TESS
2453216.6801(8)	-20299	0.0061	SuperWASP	2459857.9591(2)	-1080.5	0.0058	TESS
2453219.6169(3)	-20290.5	0.0056	SuperWASP	2459858.1320(2)	-1080	0.0059	TESS
...	...	...	...	...	...	...	...

Table 7. The N65 system's times of minima.

Min.(BJD_{TDB})	Epoch	O-C	Source	Min.(BJD_{TDB})	Epoch	O-C	Source
2453205.6882(6)	-26744	-0.0358	SuperWASP	2454076.4146(10)	-23448	-0.0302	SuperWASP
2453207.6674(5)	-26736.5	-0.0379	SuperWASP	2454076.5442(11)	-23447.5	-0.0326	SuperWASP
2453219.6897(13)	-26691	-0.0356	SuperWASP	2454076.5470(14)	-23447.5	-0.0298	SuperWASP
2453230.6506(5)	-26649.5	-0.0379	SuperWASP	2454077.3356(6)	-23444.5	-0.0339	SuperWASP
...	...	...	...	...	...	...	...

Table 8. The OT UMa system's times of minima.

Min.(BJD_{TDB})	Epoch	O-C	Source	Min.(BJD_{TDB})	Epoch	O-C	Source
2456729.3520(10)	-10257.5	-0.0558	O-C gateway	2459944.6033(1)	-85	0.0041	TESS
2456729.3523(10)	-10257.5	-0.0555	O-C gateway	2459944.7619(1)	-84.5	0.0046	TESS
2456729.3527(10)	-10257.5	-0.0551	O-C gateway	2459944.9193(1)	-84	0.0039	TESS
2456729.5096(3)	-10257	-0.0562	O-C gateway	2459945.0778(1)	-83.5	0.0044	TESS
...	...	...	...	...	...	...	...

Table 9. The PU Vir system's times of minima.

Min.(BJD_{TDB})	Epoch	O-C	Source	Min.(BJD_{TDB})	Epoch	O-C	Source
2452407.5148(50)	-31102.5	-0.0621	O-C gateway	2458050.1582(11)	-9083	-0.0367	ASAS-SN
2457174.9210(16)	-12498.5	-0.0332	ASAS-SN	2459125.4284(18)	-4887	-0.0145	ZTF
2457175.0401(10)	-12498	-0.0423	ASAS-SN	2459715.7250(10)	-2583.5	-0.0026	O-C gateway
2458050.0376(21)	-9083.5	-0.0292	ASAS-SN				

Table 10. The V0801 And system's times of minima.

Min.(BJD_{TDB})	Epoch	O-C	Source	Min.(BJD_{TDB})	Epoch	O-C	Source
2453217.6490(11)	-26426	-0.0228	SuperWASP	2454397.4671(10)	-22001.5	-0.0197	SuperWASP
2453219.6493(5)	-26418.5	-0.0224	SuperWASP	2454397.6016(10)	-22001	-0.0185	SuperWASP
2453222.7158(10)	-26407	-0.0225	SuperWASP	2454398.5324(10)	-21997.5	-0.0211	SuperWASP
2453228.7160(4)	-26384.5	-0.0219	SuperWASP	2454405.4667(7)	-21971.5	-0.0198	SuperWASP
...	...	...	...	...	...	...	...

REFERENCES

Albayrak, B., Djurašević, G., Selam, S. O., Atanacković-Vukmanović, O., & Yılmaz, M. 2005, NewA, 10, 163, doi: 10.1016/j.newast.2004.09.002

Astropy Collaboration, Robitaille, T. P., Tollerud, E. J., et al. 2013, A&A, 558, A33, doi: 10.1051/0004-6361/201322068

Avvakumova, E. A., Malkov, O. Y., & Kniazev, A. Y. 2013, Astronomische Nachrichten, 334, 860, doi: 10.1002/asna.201311942

Bellm, E. C., Kulkarni, S. R., Barlow, T., et al. 2019, PASP, 131, 068003, doi: 10.1088/1538-3873/ab0c2a

Binnendijk, L. 1970, vistas in Astronomy, 12, 217

Butters, O. W., West, R. G., Anderson, D. R., et al. 2010, A&A, 520, L10, doi: 10.1051/0004-6361/201015655

Castelli, F., & Kurucz, R. L. 2004, A&A, 419, 725, doi: 10.1051/0004-6361:20040079

Chen, X., Wang, S., Deng, L., et al. 2020, ApJS, 249, 18, doi: 10.3847/1538-4365/ab9cae

Collins, K. A., Kielkopf, J. F., Stassun, K. G., & Hessman, F. V. 2017, AJ, 153, 77, doi: 10.3847/1538-3881/153/2/77

Conroy, K. E., Kochoska, A., Hey, D., et al. 2020, ApJS, 250, 34, doi: 10.3847/1538-4365/abb4e2

Cox, A. N. 2000, Allen's astrophysical quantities (AN Cox ed)

Csizmadia, S., & Klagyivik, P. 2004, A&A, 426, 1001, doi: 10.1051/0004-6361:20040430

Damerdji, Y., Klotz, A., & Boër, M. 2007, AJ, 133, 1470, doi: 10.1086/511747

Deb, S., & Singh, H. P. 2011, MNRAS, 412, 1787, doi: 10.1111/j.1365-2966.2010.18016.x

Djurašević, G., Dimitrov, D., Arbutina, B., et al. 2006, PASA, 23, 154, doi: 10.1071/AS06016

Drake, A. J., Djorgovski, S. G., García-Álvarez, D., et al. 2014a, ApJ, 790, 157, doi: 10.1088/0004-637X/790/2/157

Drake, A. J., Graham, M. J., Djorgovski, S. G., et al. 2014b, ApJS, 213, 9, doi: 10.1088/0067-0049/213/1/9

Eggleton, P. P. 2012, Journal of Astronomy and Space Sciences, 29, 145, doi: 10.5140/JASS.2012.29.2.145

Eker, Z., Demircan, O., & Bilir, S. 2008, MNRAS, 386, 1756, doi: 10.1111/j.1365-2966.2008.13155.x

Eker, Z., Demircan, O., Bilir, S., & Karataş, Y. 2006, MNRAS, 373, 1483, doi: 10.1111/j.1365-2966.2006.11073.x

Eker, Z., Bakış, V., Bilir, S., et al. 2018, MNRAS, 479, 5491, doi: 10.1093/mnras/sty1834

Essam, A., Saad, S. M., Nouh, M. I., et al. 2010, NewA, 15, 227, doi: 10.1016/j.newast.2009.07.006

Flower, P. J. 1996, ApJ, 469, 355, doi: 10.1086/177785

Foreman-Mackey, D., Hogg, D. W., Lang, D., & Goodman, J. 2013, PASP, 125, 306, doi: 10.1086/670067

Gaia Collaboration, Montegriffo, P., Bellazzini, M., et al. 2023, A&A, 674, A33, doi: 10.1051/0004-6361/202243709

Gazeas, K., Zola, S., Liakos, A., et al. 2021, MNRAS, 501, 2897, doi: 10.1093/mnras/staa3753

Gettel, S. J., Geske, M. T., & McKay, T. A. 2006, AJ, 131, 621, doi: 10.1086/498016

Girardi, L., Bressan, A., Bertelli, G., & Chiosi, C. 2000, AAPs, 141, 371, doi: 10.1051/aas:2000126

Green, G. M., Schlafly, E., Zucker, C., Speagle, J. S., & Finkbeiner, D. 2019, ApJ, 887, 93, doi: 10.3847/1538-4357/ab5362

Guthnick, P., & Prager, R. 1933, Astronomische Nachrichten, 249, 253, doi: 10.1002/asna.19332491502

Hambálek, Ľ., & Pribulla, T. 2013, Contributions of the Astronomical Observatory Skalnate Pleso, 43, 27

Hiltner, W. A. 1962, Astronomical techniques. (University of Chicago Press)

Hoffman, D. I., Harrison, T. E., & McNamara, B. J. 2009, AJ, 138, 466, doi: 10.1088/0004-6256/138/2/466

Huang, H.-P., Yu, Y.-X., Yu, T., Hu, K., & Xiang, F.-Y. 2021, Research in Astronomy and Astrophysics, 21, 120, doi: 10.1088/1674-4527/21/5/120

Jayasinghe, T., Kochanek, C. S., Stanek, K. Z., et al. 2018, MNRAS, 477, 3145, doi: 10.1093/mnras/sty838

Jenkins, J. M., Twicken, J. D., McCauliff, S., et al. 2016, in Society of Photo-Optical Instrumentation Engineers (SPIE) Conference Series, Vol. 9913, Software and Cyberinfrastructure for Astronomy IV, ed. G. Chiozzi & J. C. Guzman, 99133E, doi: 10.1117/12.2233418

Jiang, L., Qian, S.-B., Zhang, J., & Liu, N. 2015, PASJ, 67, 118, doi: 10.1093/pasj/psv092

Khruslov, A. V. 2007, Peremennye Zvezdy Prilozhenie, 7, 6

Kopal, Z. 1959, Close binary systems (The international astrophysics series)

Kouzuma, S. 2018, PASJ, 70, 90, doi: 10.1093/pasj/psy086

—. 2023, ApJ, 958, 84, doi: 10.3847/1538-4357/ad03e1

Kreiner, J. M., Rucinski, S. M., Zola, S., et al. 2003, A&A, 412, 465, doi: 10.1051/0004-6361:20031456

Kuiper, G. P. 1941, Astrophysical Journal, vol. 93, p. 133, 93, 133

Kwee, K. K. 1958, BAN, 14, 131

Kwee, K. K., & van Woerden, H. 1956, BAN, 12, 327

Latković, O., Čeki, A., & Lazarević, S. 2021, ApJS, 254, 10, doi: 10.3847/1538-4365/abeb23

Li, K., Kim, C.-H., Xia, Q.-Q., et al. 2020, AJ, 159, 189, doi: 10.3847/1538-3881/ab7cda

Li, K., Xia, Q.-Q., Kim, C.-H., et al. 2021, AJ, 162, 13, doi: 10.3847/1538-3881/abfc53

Li, L., Zhang, F., Han, Z., & Jiang, D. 2007, ApJ, 662, 596, doi: 10.1086/517909

Lucy, L. B. 1967, ZA, 65, 89

—. 1968a, ApJ, 151, 1123, doi: 10.1086/149510

—. 1968b, ApJ, 153, 877, doi: 10.1086/149712

Malkov, O. Y., Oblak, E., Snegireva, E. A., & Torra, J. 2006, A&A, 446, 785, doi: 10.1051/0004-6361:20053137

Marsh, F. M., Prince, T. A., Mahabal, A. A., et al. 2017, MNRAS, 465, 4678, doi: 10.1093/mnras/stw2110

Masci, F. J., Laher, R. R., Rusholme, B., et al. 2019, PASP, 131, 018003, doi: 10.1088/1538-3873/aae8ac

Mitnyan, T., Szalai, T., Bódi, A., et al. 2020, A&A, 635, A89, doi: 10.1051/0004-6361/201937214

Nelson, R. H., & Robb, R. M. 2015, Information Bulletin on Variable Stars, 6134, 1

O'Connell, D. J. K. 1951, Publications of the Riverview College Observatory, 2, 85

Paki, E., & Poro, A. 2024, Astrophysics, arXiv:2405.18618, doi: 10.48550/arXiv.2405.18618

Poro, A., Blackford, M. G., Davoudi, F., et al. 2021, Open Astronomy, 30, 37, doi: 10.1515/astro-2021-0004

Poro, A., Tanriver, M., Michel, R., & Paki, E. 2024a, PASP, 136, 024201, doi: 10.1088/1538-3873/ad1ed3

Poro, A., Sarabi, S., Zamanpour, S., et al. 2022a, MNRAS, 510, 5315, doi: 10.1093/mnras/stab3775

Poro, A., Paki, E., Blackford, M. G., et al. 2022b, PASP, 134, 064201, doi: 10.1088/1538-3873/ac71cd

Poro, A., Paki, E., Alizadehsabegh, A., et al. 2024b, Research in Astronomy and Astrophysics, 24, 015002, doi: 10.1088/1674-4527/ad0866

Poro, A., Hedayatjoo, M., Nastaran, M., et al. 2024c, NewA, 110, 102227, doi: 10.1016/j.newast.2024.102227

Poro, A., Baudart, S., Nourmohammad, M., et al. 2024d, Research in Astronomy and Astrophysics, 24, 055001, doi: 10.1088/1674-4527/ad3a2c

Poro, A., Tanriver, M., Sarvari, E., et al. 2024e, Research in Astronomy and Astrophysics, 24, 045018, doi: 10.1088/1674-4527/ad30b2

Pribulla, T., Rucinski, S. M., Blake, R. M., et al. 2009, AJ, 137, 3655, doi: 10.1088/0004-6256/137/3/3655

Prša, A., Conroy, K. E., Horvat, M., et al. 2016, ApJS, 227, 29, doi: 10.3847/1538-4365/227/2/29

Qian, S. 2003, MNRAS, 342, 1260, doi: 10.1046/j.1365-8711.2003.06627.x

Qian, S. B., Wang, J. J., Zhu, L. Y., et al. 2014, ApJS, 212, 4, doi: 10.1088/0067-0049/212/1/4

Rahimi, J., Lashgari, E., Ghanbarzadehchaleshtori, M., et al. 2021, NewA, 84, 101499, doi: 10.1016/j.newast.2020.101499

Ricker, G. R., Latham, D. W., Vanderspek, R. K., et al. 2010, in American Astronomical Society Meeting Abstracts, Vol. 215, American Astronomical Society Meeting Abstracts #215, 450.06

Ricker, G. R., Winn, J. N., Vanderspek, R., et al. 2015a, Journal of Astronomical Telescopes, Instruments, and Systems, 1, 014003, doi: 10.1117/1.JATIS.1.1.014003

—. 2015b, Journal of Astronomical Telescopes, Instruments, and Systems, 1, 014003, doi: 10.1117/1.JATIS.1.1.014003

Rinner, C., Starkey, D., Demeautis, C., et al. 2003, Information Bulletin on Variable Stars, 5428, 1

Ruciński, S. M. 1969, AcA, 19, 245

Rucinski, S. M. 1992, AJ, 103, 960, doi: 10.1086/116118

—. 2000, AJ, 120, 319, doi: 10.1086/301417

Rucinski, S. M., Lu, W., Capobianco, C. C., et al. 2002, AJ, 124, 1738, doi: 10.1086/342341

Selam, S. O., Esmer, E. M., Şenavcı, H. V., et al. 2018, Ap&SS, 363, 34, doi: 10.1007/s10509-018-3252-y

Shappee, B. J., Prieto, J. L., Grupe, D., et al. 2014, ApJ, 788, 48, doi: 10.1088/0004-637X/788/1/48

Soomandar, S., & Poro, A. 2024, NewA, 105, 102112, doi: 10.1016/j.newast.2023.102112

Stassun, K. G., Oelkers, R. J., Pepper, J., et al. 2018, AJ, 156, 102, doi: 10.3847/1538-3881/aad050

Sun, W., Chen, X., Deng, L., & de Grijs, R. 2020, ApJS, 247, 50, doi: 10.3847/1538-4365/ab7894

Szalai, T., Kiss, L. L., Mészáros, S., Vinkó, J., & Csizmadia, S. 2007, A&A, 465, 943, doi: 10.1051/0004-6361:20066768

Terrell, D., Gross, J., & Cooney, W. R. 2012, AJ, 143, 99, doi: 10.1088/0004-6256/143/4/99

Terrell, D., & Wilson, R. E. 2005, Ap&SS, 296, 221, doi: 10.1007/s10509-005-4449-4

Tian, X.-M., Zhu, L.-Y., Qian, S.-B., Li, L.-J., & Jiang, L.-Q. 2018, Research in Astronomy and Astrophysics, 18, 020, doi: 10.1088/1674-4527/18/2/20

Tody, D. 1986, in Society of Photo-Optical Instrumentation Engineers (SPIE) Conference Series, Vol. 627, Instrumentation in astronomy VI, ed. D. L. Crawford, 733, doi: 10.1117/12.968154

Tonry, J. L., Denneau, L., Flewelling, H., et al. 2018, ApJ, 867, 105, doi: 10.3847/1538-4357/aae386

Torres, G. 2010, AJ, 140, 1158, doi: 10.1088/0004-6256/140/5/1158

Weldrake, D. T. F., Sackett, P. D., Bridges, T. J., & Freeman, K. C. 2004, AJ, 128, 736, doi: 10.1086/422433

Yakut, K., & Eggleton, P. P. 2005, ApJ, 629, 1055, doi: 10.1086/431300

Yıldırım, M. F. 2022, Research in Astronomy and Astrophysics, 22, 055013, doi: 10.1088/1674-4527/ac5ee8

Yıldız, M. 2015, Research in Astronomy and Astrophysics, 15, 2244, doi: 10.1088/1674-4527/15/12/012

Zhang, X.-D., & Qian, S.-B. 2020, MNRAS, 497, 3493, doi: 10.1093/mnras/staa2166

Zola, S., Gazeas, K., Kreiner, J. M., et al. 2010, MNRAS, 408, 464, doi: 10.1111/j.1365-2966.2010.17129.x